Fused filament fabrication of scaffolds for tissue engineering; how realistic is shape-memory? A review

Marie Bayart, Sébastien Charlon, Jérémie Soulestin

Fused filament fabrication of scaffolds for tissue engineering; How realistic is shape-memory? A review

Marie Bayart[1], Sébastien Charlon[1*], Jérémie Soulestin[1]

[1] IMT Lille Douai, École Nationale Supérieure Mines-Télécom Lille Douai, Materials & Processes Center, Cité Scientifique, Villeneuve d'Ascq Cedex, France

[*] corresponding author: sebastien.charlon@imt-lille-douai.fr

IMT Lille-Douai, Bâtiment plasturgie, 764 Boulevard Lahure, 59500 Douai, France

Abstract

Since the invention of additive manufacturing (AM) in the 1980s, great advances are today conceivable thanks to considerable evolution in recent years. Medicine, and particularly tissue engineering (TE), have high expectations regarding AM, which allows the manufacturing of complex personalized parts. Among existing techniques, fused filament fabrication (FFF) is very promising in the biomedical field, due to its many advantages, particularly for specific applications such as scaffolds for TE. This review, in interaction with biomedical, process and material sciences, aims to help researchers understand the importance of process parameterization (build orientation, raster angle, layer thickness, etc.) combined with an appropriate material choice, to develop optimized scaffolds using FFF. This review also reflects the state of existing advances and opens perspectives on the subject, especially with the use of biodegradable and biocompatible shape-memory polymers, the principle of which will be revisited and the few studies concerning shape-memory scaffolds will be gathered.

Keywords: Additive manufacturing (AM); fused filament fabrication (FFF); scaffolds; shape-memory polymers (SMPs); 4D printing

Nomenclature

ABS: acrylonitrile butadiene styrene
AM: additive manufacturing
EBM: electron beam melting
FFF: fused filament fabrication
HA: hydroxyapatite
HDPE: high-density polyethylene

HIPS: high-impact polystyrene

MSC: mesenchymal stem cell

PA: polyamide

PBS: phosphate-buffered saline

PCL: polycaprolactone

PDLLA: poly (D,L-lactic acid)

PE: polyethylene

PEEK: polyether ether ketone

PEG: poly (ethylene glycol)

PEI: polyetherimide

PELA: poly (D,L-lactic acid-*co*-ethylene glycol-*co*-D,L-lactic acid)

PGA: poly (glycolic acid)

PHAs: polyhydroxyalkanoates

PLA: poly (lactic acid)

PLGA: poly (lactic-*co*-glycolic acid)

PLLA: poly (L-lactic acid)

PMMA: poly (methyl methacrylate)

PP: polypropylene

PS: polystyrene

PU: polyurethane

PVA: poly (vinyl alcohol)

PVC: poly (vinyl chloride)

SLA: stereolithography

SLM: selective laser melting

SLS: selective laser sintering

SM: shape memory

SME: shape-memory effect

SMP: shape-memory polymer

TCP: tricalcium phosphate

TE: tissue engineering

TPU: thermoplastic polyurethane

UHMWPE: ultra-high-molecular-weight polyethylene

UTS: ultimate tensile strength

Introduction

Additive manufacturing (AM) is defined in the ISO/ASTM 52900 standard as "process of joining materials to make parts from 3D model data, usually layer upon layer, as opposed to subtractive manufacturing and formative manufacturing methodologies" [1]. Several different AM techniques are commercially available and share common advantages like the possibility to design devices for small-scale manufacturing at a low price in contrast to usual processing techniques such as injection molding, whose equipment costs (e.g. expensive molds for each part) must be made cost-effective by large-scale production. AM is a time-saver for rapid prototyping and for personalized applications, and it also limits raw material waste as compared to subtractive manufacturing processes. Finally, AM allows the designing and printing of very complex structures that are not always achievable with traditional processing techniques [2].

With this in mind, AM appears very interesting for the biomedical field as each patient is unique and should have access to products adapted to their needs. It is even truer in the precise field of tissue engineering (TE) and regenerative medicine, which is one of the major topics of research. Indeed, most tissues are able to recover from minor damages only. For example, bones have natural means of renewal and strengthening through the joint action of osteoclasts and osteoblasts [3]. However, their capacity of renewal is limited in the case of severe damage and tissues require medical intervention to repair, regenerate and strengthen. This could be done thanks to the development of scaffolds and progress in TE. Scaffolds are meant to provide a structure for cells to attach, to proliferate and differentiate. Traditional techniques for scaffold production include solvent casting [4,5], electrospinning [6,7], particulate/salt leaching [4,8], supercritical gas foaming [9] and so on. Still, these techniques can somehow be unpredictable in terms of porosity control, while thanks to AM, processing parameters could be chosen in order to obtain precise and reproducible structures and porosity.

Techniques of AM used in biomedical fields include selective laser sintering (SLS), selective laser melting (SLM), electron beam melting (EBM), fused filament fabrication (FFF) and stereolithography (SLA) [10]. They differ in the transformation of the raw material into a succession of layers. SLS, SLM, EBM and FFF partially or totally melt the raw material (powder, pellets, filament) while SLA cures a liquid resin [11]. FFF appears attractive since the equipment and its maintenance are quite inexpensive and FFF is an easy-to-use AM

technique [12,13]. It also requires lower cost materials (e.g. thermoplastic filament) than most of the other techniques.

Of all thermoplastic polymers, their potential to be printed and, then, to be implanted in the human body are critical points. From the technical side, adequate rheological and thermo-physical properties are essential. Duty *et al.* developed a model to assess material "printability" and identify adequate processing conditions [14]. From the biological side, biocompatibility and bioactivity are obviously necessary characteristics. A synthetic scaffold is also meant to be degraded simultaneously with the development of new tissues, without releasing toxic compounds.

Finally, shape-memory polymers (SMPs) were recently introduced to avoid invasive surgery. Indeed, SMPs permit the production of small parts (small temporary shapes) to limit the size of the surgical incision and to facilitate their insertion into damaged tissues. The parts then deploy thanks to an intrinsic stimulus (e.g. temperature, moisture) after implantation and recover their permanent shape. This feature could be very interesting to produce scaffolds for regenerative medicine.

Many reviews gather pieces of information about the different 3D printing techniques for biomedical applications [15–20], AM of shape-memory materials for biomedicine [18,21,22], biomaterials for scaffolds produced with traditional techniques and the interactions between scaffolds and cells [20,23–26] but to the best authors' knowledge, no review focuses on the peculiar FFF technique to produce biodegradable and shape-memory scaffolds for TE. For these reasons, the aim of this work is to show that FFF has great potential for the production of scaffolds for TE and permits to overcome the problems encountered with traditional techniques. In addition, it enables to print SMPs (4D printing). Required material characteristics for body implantation will first be summarized. Then, the FFF process, its advantages and adequate settings for scaffolding will be discussed. The last section will introduce SMPs to conclude with scaffold 4D printing.

I. Required polymer characteristics to manufacture scaffolds for TE

I.1. Biocompatibility

The most important characteristic of a polymer intended to be in contact with or implanted in the human body is its biocompatibility. Initially synonymous with inert, that is, not inducing a reaction from the organism, the term "biocompatible" has evolved. Now, biocompatibility

also includes the ability of the material to obtain a positive response from the organism with a minimal inflammatory reaction. A wide range of biocompatible and/or natural polymers is used or is being investigated to be used in biomedical applications (Table 1).

Table 1 Biocompatible polymers and copolymers and their current/potential biomedical applications

Category	Polymer/Copolymer	Applications	Ref
Polyesters	PLA	Sutures, scaffolds for TE, drug delivery	[27–29]
	PGA		
	PLGA		
	PCL		
	PHAs		
Polyurethanes	PU	Bioadhesives, dentistry, breast implants, orthopedics, cardiovascular devices, wound dressing, tissue reconstruction, contraception	[30]
Polyolefins	PE, HDPE, UHMWPE	Bone replacement, tubing, packaging films	[31–34]
	PP	Sutures, mesh, orthopedics, syringes, catheters	[35,36]
Polyamides	PA 12, PA 6, PA 66, PA 612	Bone scaffolds, tubing, catheters, surgical instruments, sutures	[34]
Vinyl polymers	PVC	Tubes, blood bags, disposable medical devices	[37]
	PVA	Drug delivery, wound dressing	[38,39]
Styrene polymers	PS, HIPS	Tissue culture trays, petri dishes, test tubes, catheter trays, heart pump trays, epidural trays, respiratory care equipment, syringe hubs, suction canisters	[34]
Acrylic polymers	PMMA	Intraocular lens, dental and mandibular corrections, bone cement	[40,41]
Polyaryletherketones	PEEK	Spinal, orthopedic and maxillofacial surgery	[42,43]
Natural polymers	Collagen, chitosan, alginate, cellulose	Drug delivery, implants for TE (scaffolds, skin replacement, bone substitutes, artificial blood vessels and valves), wound healing	[44–48]

HDPE=high-density polyethylene; HIPS= high-impact polystyrene; PA=polyamide; PCL=polycaprolactone; PE=polyethylene; PEEK=polyether ether ketone; PGA=poly (glycolic acid); PHAs=polyhydroxyalkanoates; PLA=poly (lactic acid); PLGA=poly (lactic-co-glycolic acid); PMMA=poly (methyl methacrylate); PP=polypropylene; PS=polystyrene; PU=polyurethane; PVA=poly (vinyl alcohol); PVC=poly (vinyl chloride); UHMWPE=ultra-high-molecular-weight polyethylene

However, for scaffolding, some of these polymers are more suitable than others and additional properties (e.g. bioactivity, biodegradability, mechanical properties) are needed to meet the TE requirements. Copolymers, polymer blends [29] and composites with bioactive components are often produced to obtain these properties. Bernard *et al.* published a comprehensive review regarding the biocompatibility of polymer-based materials for medical devices containing precious information about the standards and regulations for biological evaluation [49].

I.2. Bioactivity

Bioactive materials stimulate the biological response of the body. Chemical (e.g. surface hydrophilicity), physical (e.g. surface roughness, Young's modulus) improvements, or both can generate bioactivity.

Calcium phosphate ceramics such as hydroxyapatite (HA) $Ca_{10}(PO_4)_6(OH)_2$ and tricalcium phosphate in its β form (β-TCP) $Ca_3(PO_4)_2$ are often used as bioactive fillers [4,31,32,50–53]. HA is highly biocompatible, osteoconductive and is similar to biological apatite (main constituent of enamel, dentin and bone) [54]. Marra *et al.* used formulations of HA and PCL/PLGA to produce scaffolds and highlighted viable cells and formation of collagen 500 µm deep into the scaffold containing 10 wt.% of HA [8]. Jeong *et al.* produced PLA/HA (5 wt.% and 20 wt.%) scaffolds by electrospinning and revealed viable cells and continuous cell proliferation for 21 days [6]. They concluded that their scaffolds were effective to grow pre-osteoblasts (for bone regeneration). β-TCP also demonstrates inherent biomimetic potential and can be used as a bioactive filler in scaffolds for TE [55]. It has the advantage over HA of being much more soluble in biological media [56]. However, β-TCP is less advantageous in terms of mechanical properties and HA and β-TCP are sometimes combined to achieve better flexural strength and fracture toughness with HA and higher biodegradability with β-TCP [57]. HA and β-TCP have also proved to increase surface roughness and thus, cell attachment, proliferation, differentiation and tissue mineralization [5,58]. Other fillers such as bioactive glasses (silicate glasses and glass-ceramics) can induce strong bonding between hard and soft tissues and are of particular interest for TE [59]. In Serra *et al.*'s study, surface roughness increased from 117.72 ± 60.50 nm for PLA to 1003.89 ± 228.45 nm for PLA-glass (50 wt.%) [60,61].

Altankov and Groth pointed out that mammalian cells' interaction with materials was better when their surface was hydrophilic than in the case of non-wettable surfaces [62]. They observed a high proliferation of fibroblasts on hydrophilic clean glass whereas on octadecyl glass, which is hydrophobic, no cell growth occurred. Hydrophilicity can also be tuned by choosing the right material composition. For instance, PLGA is known to be more hydrophilic than other polyesters such as poly (L-lactic acid) (PLLA), and hydrophilicity of their blends can be tuned by varying PLLA/PLGA ratios [63]. Kao *et al.* used polydopamine to coat PLA scaffolds and found that it greatly increased their hydrophilicity. They observed reduced contact angles from 130° for the pure PLA scaffold to lower than 51.9° and 0° (totally

hydrophilic) for the coated ones with increasing dopamine content in the coating solution (from 1 to 2 mg/mL in 10 mM Tris, pH 8.5) [64]. They showed that polydopamine helped to promote the proliferation of human adipose-derived stem cells and increased collagen I, cell cycle, and cell adhesion. Wang *et al.* used cold atmospheric plasma to functionalize the surface of PLA scaffolds for bone regeneration and showed that this treatment improved the surface of their samples both physically and chemically [65]. Indeed, the water contact angle measured on the surface of the scaffolds decreased from 70 ± 2° to 24 ± 2° and the nano-scale surface roughness increased from 1.2 nm to a maximum of 27.6 nm. As a result, it promoted both osteoblast and mesenchymal stem cell (MSC) attachment and proliferation.

Certain properties such as surface roughness can also be adjusted by selecting suitable processing parameters. This will be discussed in a later section.

I.3. Biodegradability

Some polymers have the advantage of being biodegradable. Such polymers could be implanted in the body and be automatically eliminated after an adequate time, thus avoiding a second surgical intervention to remove the implant. Polyesters and natural polymers presented in Table 1 can biodegrade in certain conditions. PLA, PGA and PCL are biodegradable polyesters that are already well implanted in the biomedical field and formulations containing PLA, PGA and PCL have already been approved by US and European agencies [18,66–68].

Their biodegradation is dependent on several factors and can be tuned, for example, by controlling their molecular weight [69]. In the particular case of PLA, chirality influences its biodegradation rate. The presence of D and L/D forms are known to increase the rate of degradation of PLA [70]. Actually, crystallinity, directly related to the chirality of PLA, has a huge impact on degradation. Amorphous regions degrade faster than crystalline ones, so that tuning the material crystallinity induces changes in its degradation kinetics [25,71]. Chen *et al.* mention that blending PLLA with poly (D,L-lactic acid) (PDLLA) can increase the kinetics of degradation of the final compound thanks to the amorphous nature of PDLLA [72].

PLGA (a copolymer of PLA and PGA) is the most studied biodegradable polymer for biomedicine because its properties can easily be tuned for specific applications by choosing the right lactic/glycolic molar ratio [71]. To determine the rate of degradation and the different steps of degradation of PLGA (different formulations) scaffolds, Wu and Ding used a phosphate-buffered saline (PBS) solution at 37°C, in order to mimic the natural body environment [73]. They measured the properties of PLGA (85/15 and 75/25) and PDLLA

scaffolds at different times after immersion in the solution. Their results showed that the PLGA 85/15 scaffold of higher molecular weight resisted degradation longer than the 75/25, while the PDLLA scaffold stayed almost intact after 26 weeks. Peng *et al.* used PLGA to adjust the degradation rates of PCL/PLGA scaffolds, as PCL has the advantage of being flexible but has a slow degradation rate and quite low bioactivity [74]. They showed that the addition of PLGA drastically increased the kinetics of degradation because of PLGA hydrophilicity. According to them, the 0.5PCL/0.5PLGA scaffold presents the ideal degradation rate so that degradation and cell growth, and tissue maturation match (alveolar bone).

PUs are also materials of choice for biomedical implants and Santerre *et al.* devoted an entire review to the subject of their biodegradation [75].

Finally, the architecture of a whole device influences its rate of degradation. Bosworth and Downes summarized the two schools of thought regarding this aspect [76]. The first is that porous structures have more specific surface area and degrade faster than dense structures, because of the facility for water molecules to penetrate them. The second is that porous structures permit better evacuation of acidic products, decreasing autocatalysis. Results from their own study on degradation of PCL scaffolds in PBS at 37°C tend to support the first assumption that higher surface area to volume ratio induces faster degradation. A process allowing a good control of the porosity seems therefore appropriate to tailor the degradation kinetics of biomedical devices.

II. Fused filament fabrication (FFF)

II.1. Principle

Each AM technique needs to start from the design of a 3D part using computer-aided design or imaging techniques such as magnetic resonance imaging, computed tomography scans, etc. The resulting file (.stl) is then loaded in a slicing software to transform the 3D designed part into a layered structure and to generate a file in “G-code”, which is a common programming language to define a toolpath. The AM machine then reads this file, containing essential information like the layer thickness or the deposition angle, and manufactures the 3D part.

FFF is based on extrusion that consists of melting/plasticizing raw materials in an extrusion head moving in the x and y directions. The molten material is pushed out of a nozzle to form a filament, which is deposited on a build plate to participate in the formation of a layer, thanks to the movements of the extrusion head governed by the G-code file. Once the first layer is

completed, the build plate moves down in the z direction for a distance equal to the layer thickness and the deposition of the second layer starts. This cycle is reproduced until the complete fabrication of the part, which can be of very complex shape, as seen in Figure 1. Although the raw material is usually a thermoplastic polymer or a composite with a thermoplastic matrix (*e.g.* PLA and hydroxyapatite particles [58]) in the form of filament spools (Figure 2), a few innovative AM machines now allow the use of pellets (Freeformer from Arburg, Germany; Pam Series P from Pollen AM, France, David from Sculptify, USA, etc.).

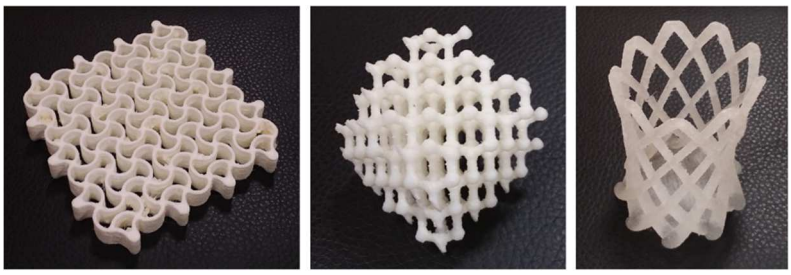

Figure 1 : Complex shapes manufactured with an Arburg Freeformer (FFF)

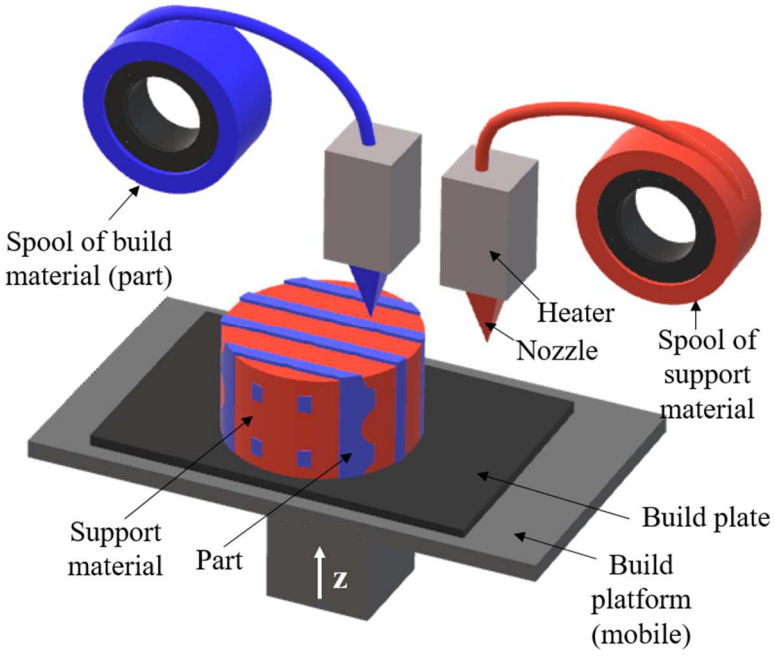

Figure 2 : Schematic FFF process

Post-treatments of the resulting parts are sometimes required. For instance, a post-treatment is necessary when the part is printed with support material (also called sacrificial material) that has to be removed (Figure 3). With FFF machines equipped with two extrusion heads, the support material is different from the material constituting the part. In certain cases, it can be

dissolved in a specific solvent, such as water to dissolve PVA. With FFF machines equipped with only one extrusion head, the support material, printed in the same material as the part, has to be mechanically removed. To facilitate this step, support material structures are printed with a lower density than the part.

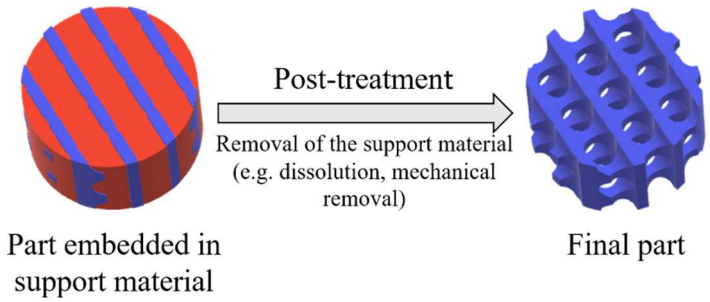

Figure 3 : Post-treatment of a part; support material removal

In some cases, post-treatments are required to decrease the surface roughness. For example, Garg *et al*. exposed acrylonitrile butadiene styrene (ABS) FFF-printed parts (with different orientations) to cold vapors of acetone and showed that this treatment was very efficient [77]. For instance, they reached a surface roughness of 2.5 µm with chemical treatment compared to 6.27 µm before treatment for the 15°-oriented part, with minimal variations in the geometric accuracy of the part. The applications considered by the authors were obviously not targeted for biomedical applications, since high surface roughness tends to promote cell adhesion.

Although FFF is very easy to handle to produce complex parts, it also has several drawbacks. Compared to parts produced with traditional polymer processes, FFF-printed parts tend to have lower mechanical properties because of their internal structure consisting of a succession of filaments and layers. The deposition angles induce anisotropy in the part, and the cylindrical geometry of the filament limits contact between adjacent filaments, which tends to create intrinsic porosity and thus, to weaken the mechanical properties of the part. Additionally, the mechanical properties of an FFF-printed part depend on the adhesion strength between adjacent filaments that is led by the process parameters. The deposition of warm layers onto cold ones creates thermal stresses, promoting negative phenomena like shrinkage and warping effects and the delamination of adjacent layers. That is why, the choice of adequate printing parameters is a key point.

II.2. Optimization of the FFF process

II.2.1. For dimensional accuracy

Polymers should have suitable rheological and viscoelastic properties to be well transformed by FFF and to reach shape and dimension stability during the entire process, meaning that shrinkage and warpage should be avoided or limited as far as possible [14]. Shrinkage and warpage can usually be minimized by using amorphous materials [78] as crystallization induces volume reduction and undesired effects [79], by controlling the temperature of the manufacturing chamber, the nozzle and the bed, and/or by mixing the polymer with fillers. Wu *et al.* minimized the warpage of PEEK samples by choosing the right chamber (130°C) and nozzle (350°C) temperatures [80]. The warping deformation decreased from 1.93 mm to 0.65 mm by increasing the chamber temperature from 90°C to 130°C. They attributed the warpage to uneven crystallization occurring during rapid cooling, causing high internal stress, and they concluded that the chamber temperature had more influence on warpage than the nozzle temperature. Spoerk *et al.* revealed that a chamber temperature of 55°C (compared to 25°C) permitted to decrease internal stress in PP-borosilicate parts [81]. Indeed, during printing, the part is submitted to the chamber temperature for a certain time. This is equivalent to annealing, which releases stress and gives the material more time to crystallize. As a result, parts printed in warmer construction environments tend to be less subject to geometric variations after printing. Wang *et al.* showed the absence of warping deformation when the chamber temperature was equal to the glass transition temperature (T_g) of the polymer [82]. However, a balance must be found to minimize warpage but still enable layer solidification. That is why, even though the T_g of ABS is close to 104°C, the chamber temperature (or envelope temperature) is often lower (e.g. 70°C [83]; 75°C [84]).

Fillers are often used to reduce shrinkage and to control warpage [85]. Kochesfahani studied different formulations of PLA and minerals (talc, calcium carbonate, mica, kaolin etc.) to be processed via FFF [86]. The results revealed that minerals reduced shrinkage, warpage and improved the thermal stability of PLA. In some cases, minerals permitted to anneal the parts without losing their original shape and to reach maximum crystallinity at a reasonable speed, thanks to a better nucleation.

II.2.2. For surface properties

Regarding the surface aspect, in general, a small layer thickness induces a low surface roughness, and adjusting processing parameters such as the part orientation during its production can influence the well-known staircase effect [13]. Depending on the application,

a high or low surface roughness may be preferred and layer thickness, surface slopes, deposition angles, types of support and filling methods were shown to have an impact on it. Both experimental and simulation studies allow to adjust the processing parameters as a function of the desired properties [87,88]. The nozzle temperature also has an impact on surface roughness, as revealed in Chaidas *et al.*'s study [89]. They measured the surface roughness (average mean surface roughness Ra, surface roughness depth Rz, total height of the roughness profile Rt and arithmetic mean width of profile elements Rsm) of PLA samples printed with different nozzle temperatures and found that the increase in the temperature induced decreases in all the roughness parameters (Ra, Rz, Rt and Rsm). In a similar study, Wang *et al.* explained that higher temperatures enabled higher molecular movement and thus, better diffusion, and managed to model the surface roughness as a function of printing parameters [90].

II.2.3. For mechanical properties

Many parameters can have an impact on the mechanical properties of an FFF printed part. Figure 4 illustrates certain parameters that can be set on the machine and some features resulting from the machine settings.

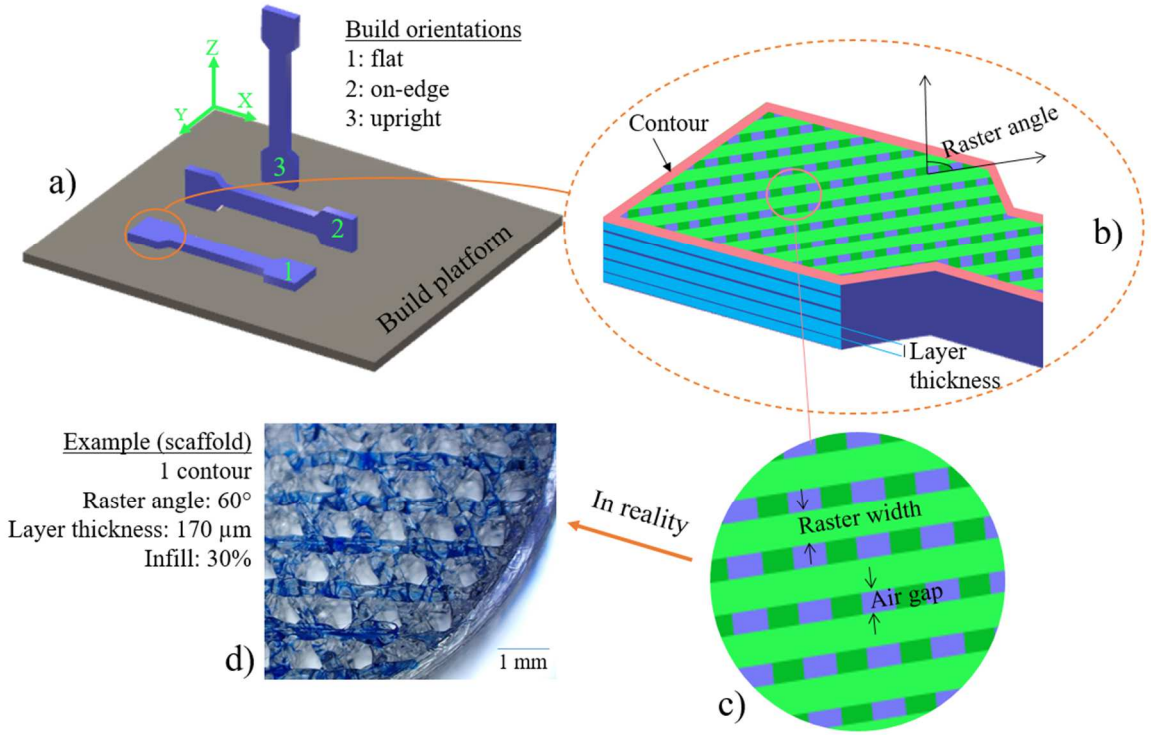

Figure 4 : a) Different build orientations; b) Tunable parameters; c) Raster width and air gap; d) Example of an FFF-printed scaffold and its printing settings

The FFF process is well known to create anisotropic mechanical properties in the three directions of printed parts. Actually, Chacón *et al.* studied the effect of the build orientation on the mechanical properties of PLA samples [91]. They built samples upright, on-edge and flat on the platform, resulting in different mechanical performances. Flat and on-edge samples showed the highest mechanical properties (tensile and flexural strengths and stiffness) and ductile trans-layer failure. On the contrary, upright samples showed the lowest mechanical properties (e.g. tensile strength 78% to 37% lower than on-edge and flat orientations with different printing parameters). Indeed, during tensile testing, the weakest inter-layer bonds are solicited for upright samples, which showed brittle intra-layer failure. Rodríguez-Panes *et al.* revealed that increasing the infill (i.e. smaller air gap) resulted in denser specimens with less porosity and thus, higher mechanical strength [92]. Popescu *et al.* reviewed more than 49 papers about the influence of FFF parameters and their interactions on the mechanical properties of various printed parts [93]. They concluded that the most significant changes were governed by the air gap (mechanical properties enhanced with a reduced or even negative air gap), the build orientation, the raster angle, the layer thickness (small layer thickness increasing the mechanical strength) and the infill percentage.

From a thermal point of view, Faes *et al.* quantified the influence of the inter-layer cooling time (*i.e.* the time between the deposition of two consecutive layers) on the mechanical properties of ABS parts printed by FFF [94]. They found that a longer inter-layer cooling time induces weaker bonding and thus, decreases the mechanical properties (Young's modulus, ultimate tensile strength (UTS) and elongation at break) when the part is built in the upright direction. For example, the UTS of the upright samples decreased from 20.5 MPa to 13.3 MPa when the inter-layer cooling time increased from 3.59 s to 45.27 s. This was not observed for the flat samples whose UTS remained constant (19 MPa) while the inter-layer cooling time increased from 54.92 s to 282.71 s. Indeed, when parts are printed upright and tested in tension, their inter-layer bonds are loaded, whereas for flat samples, the intra-layer bonds are solicited (stronger than the inter-layer bonds). Process temperatures also have a great effect on the mechanical properties of the printed parts. Shelton *et al.* proved that the chamber temperature conditions the envelope temperature, which is defined as the ambient temperature around the printed part [95]. They varied the envelope temperature from 110°C to 170°C and determined a 20% higher UTS for the sample made of ULTEM™ 9085 resin with an envelope temperature of 170°C compared to the sample with an envelope temperature of 110°C. They explained this improvement of the UTS by an increased neck development at

higher temperature. Garzon-Hernandez *et al.* represent neck formation as follows in Figure 5 [96].

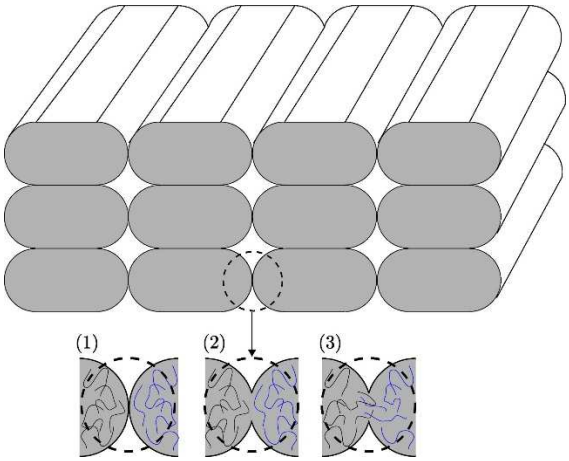

Figure 5 : Formation of a neck between filaments (1) surface contact; (2) neck growth; (3) neck growth and molecular diffusion at the interface. Reprinted with permission from Ref. [96], copyright (2020), Elsevier.

Many studies and reviews were found in literature about the influence of different parameters on the mechanical properties of various printed parts [91,93–95,97,98] and a few studies even developed methods to predict the mechanical properties of a part by knowing the parameters used [96].

To sum up, FFF seems to be a promising process to manufacture specific and personalized objects for biomedical applications since it has many advantages and few drawbacks, which can be limited by setting optimization. The main limitation to the use of FFF in the biomedical field is the lack of existing pharmaceutical grade polymers with the appropriate properties to be printed with this technique [99]. Indeed, entire studies and reviews focus on the influence of FFF processing parameters on mechanical properties of printed parts, degree of bonding, and many other properties, but biocompatible and biodegradable polymers (with the exception of PLA) are rarely found in the literature (generally ABS, polyetherimide (PEI), PEEK). However, even though these current materials do not have the same properties as polymers used for biomedical applications, the influence of the above-mentioned parameters should follow the same trends. Also, Popescu *et al.* point out that further research should evaluate the mechanical performances of FFF parts for specific applications (e.g. scaffolds) and not only test specimens [93].

III. FFF for scaffolding

III.1. Potentially adequate materials for scaffold printing (FFF)

A few articles evaluate the performance of scaffolds manufactured by FFF. Among these works, PLA is often studied because it has the required characteristics to be used in biomedical applications and in AM processing [100,101]. PLA has a melting temperature close to 160°C [102] and shows good dimensional stability and good adhesion to build platforms, meaning that it does not need to be printed on a heated build platform [92,103]. Its printing temperature range is rather low and Shahriar *et al.* estimated it was 160°C-190°C with a maximum value of bonding length at 167°C (measured with two adjacent filaments in an oven) [102]. Nevertheless, it is not rare to find higher printing temperatures in literature such as in Grasso *et al.*'s work, where PLA is printed at 215°C [104]. Drummer *et al.* studied the suitability of PLA/TCP for FFF and concluded that this composite material could be used to print scaffolds for TE [78]. Amorphous PCL is also commonly used because of its low T_g close to -60°C and its high thermal stability (decomposition temperature of 350°C compared to 235°C-255°C for other aliphatic polyesters tested), making it easy to print without degradation [105,106]. Most importantly, PCL has very suitable rheological and viscoelastic properties, facilitating its extrusion and enhancing its processability [18]. PLGAs are thermolabile, which means that processing at high temperature such as during FFF can provoke thermal degradation [107], the formation of toxic component and unpredictable behavior in the human body since the integrity of the material can be altered [108]. PLGAs integrity is highly reliant on the residence time during processing [109] and depending on their lactic/glycolic molar ratio (higher lactic content increasing thermo-oxidative stability [110]), PLGAs might not always be well suited for FFF. Still, some research proved the feasibility of using PLGAs for scaffolding via FFF [107,111].

Many other polymers should be tested (Table 1) to evaluate the whole potential of scaffolds manufactured by FFF.

III.2. Scaffold optimization

The aim of scaffolds is to provide space and a support structure for cells to infiltrate, attach, proliferate (Figure 6) and produce new extracellular matrix.

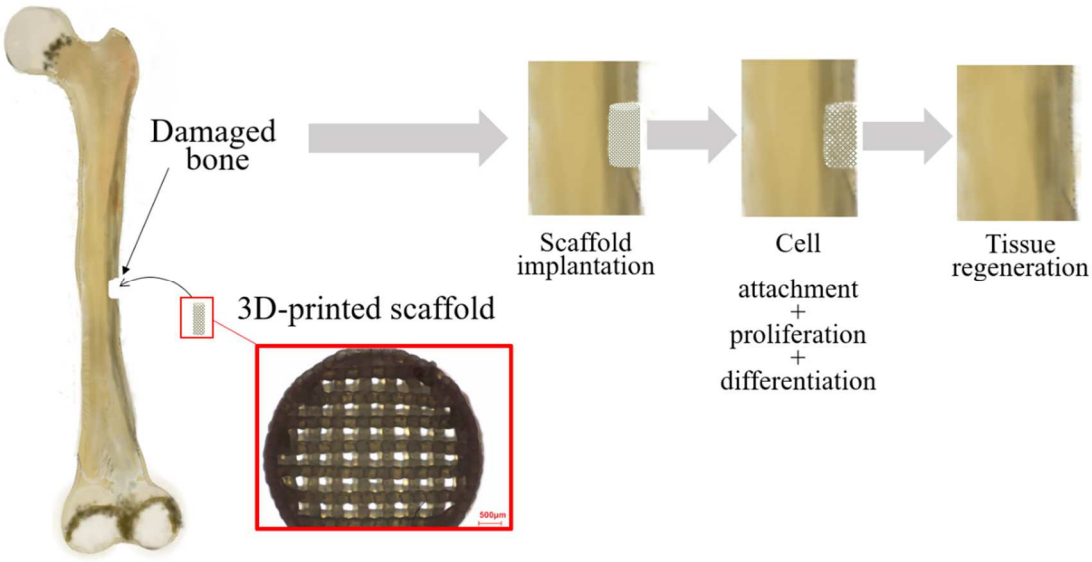

411

412 *Figure 6 : Representation of a 3D printed (FFF) scaffold for bone regeneration*

413 To do so, they need to possess specific properties such as biocompatibility, bioactivity, and
414 biodegradability, as discussed earlier. Other properties, such as high enough mechanical
415 properties (rigidity, resistance to impact and to friction, etc.) matching those of the tissues
416 meant to be colonized, are essential to maintain the structure after implantation. Porosity
417 features are also of great importance for tissue ingrowth and vascularization. The effect of
418 different pore sizes has already been reviewed in detail [112] as well as materials for scaffold
419 production, required structure, and mechanical properties of human tissues [113]. Some of
420 these properties directly result from the materials used but some result from the structure of
421 the medical device (scaffold), sometimes induced by the processing technique. In the
422 particular case of FFF, various architectures can be obtained (examples given in Figure 7) and
423 induce different cell behaviors.

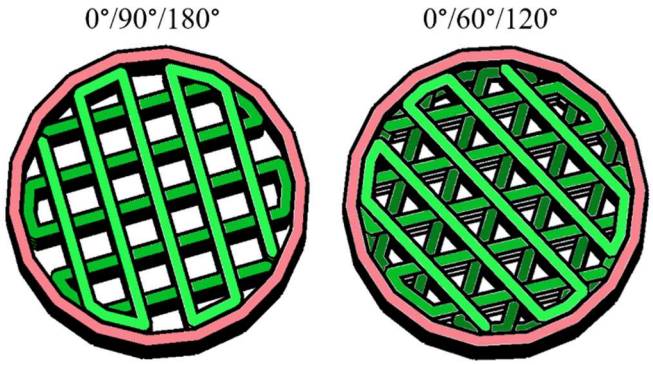

424

425 *Figure 7 : Examples of scaffold architectures induced by different raster orientations*

Zein *et al.* studied several different FFF printed scaffold architectures, compared their properties and showed that they could be significantly impacted by the processing parameters [106]. Indeed, all the scaffolds were printed with the same material, namely PCL, but differences in their architecture were generated by variation in the filament width, porosity or lay down pattern (raster orientations). These induced properties such as a compressive stiffness varying from 4 MPa to 77 MPa, a yield strength from 0.4 MPa to 3.6 MPa and a yield strain from 4% to 28%. With the same value of porosity, raster orientations of 0°/90°/180° and 0°/60°/120° induced differences in the mechanical properties of the scaffolds. According to Ostrowska *et al.*'s study, repetitive 0°/60°/120° raster orientation globally leads to a high elastic modulus and the highest shear storage modulus as compared to 0°/15°/30°, 0°/30°/60°, 0°/45°/90°, 0°/75°/150° and 0°/90°/180°, and is one of the most commonly used orientations in the treatment of bone diseases [114]. Differences can be explained by the number of filament connections between layers (higher for 0°/90°/180° and 0°/60°/120°) and pore shape. For instance, square shape (0°/90°/180° orientation) is associated to a low shear storage modulus. Ostrowska *et al.* took their research a step further by analyzing the effect of their PCL scaffold architecture on cell seeding, proliferation and osteogenic differentiation. 0°/15°/30° structure presented a higher cell number after 8 hrs since the tortuous architecture of this scaffold helped trap the cells and enabled better seeding. However, after 35 days, the architecture 0°/60°/120° displayed the highest cell number. They found only slight variations in the differentiation of MSC on their constructs.

In most studies, though, researchers adjust both the FFF parameters and the scaffold composition to achieve optimal properties. Bruyas *et al.* made a very complete study on processing parameters and scaffold composition to print PCL/β-TCP scaffolds [55]. For instance, they varied the strut distance (air gap), that influenced porosity, and measured the mechanical properties under compression of scaffolds of different compositions. They concluded that porosity was mostly dependent on the strut distance (more porous with longer strut distance), whereas the β-TCP amount had only little influence. They measured Young's modulus values varying from 12 MPa (highest strut distance and highest β-TCP amount) to 188 MPa (lowest strut distance and highest β-TCP amount), and yield strength values from 0.7 MPa (highest strut distance and highest β-TCP amount) to 15.4 MPa (lowest strut distance and lowest β-TCP amount). According to them, the amount of β-TCP does not influence the Young modulus in the case of high porosity scaffolds while increasing the amount of β-TCP increases the Young modulus in the case of low porosity scaffolds. Regarding the yield

strength, the strut distance has clearly more influence than the composition of the scaffolds. Composition, however, had a major effect on other properties. Indeed, β-TCP greatly increased the surface roughness of the scaffolds (178.3 ± 67.6 nm, 645.7 ± 84.7 nm, 1193.6 ± 97.6 nm, and 1837.6 ± 317.6 nm for β-TCP ratios of 0%, 20%, 40%, and 60%, respectively). They performed accelerated ageing (alkaline conditions) and demonstrated that increasing the amount of β-TCP in the composites tremendously accelerated degradation (less than 20 hrs to fully degrade the 60% filled composite as compared to <1% weight loss for pure PCL after 54 hrs). These differences in properties induced various cellular behaviors. After 11 days of the proliferation study, the number of cells was about 50% higher on the scaffolds that contained β-TCP. β-TCP also had a great impact on osteogenic differentiation and 40% and 60% formulations revealed an increase in the alkaline phosphatase activity at day 11.

Many examples of scaffold compositions for TE produced by FFF with several different processing parameters and scaffold behavior toward cells were found in the literature and gathered in Table 2.

Table 2 : Non-exhaustive list of scaffolds manufactured for TE printed via FFF and their main characteristics (Tn=nozzle temperature, Tp=platform temperature, Ø=diameter)

Materials	Process parameters Device main features	Applications	Main results	Ref
PLA-based scaffolds				
PLA	Tn: 195°C Nozzle Ø: 500 µm Pore size: 350 µm Strut diameter: 700 µm Porosity: 40%	Scaffold for bone TE	The pore size and strut diameter measured were very close to the design values (350±80 µm and 700±120 µm, respectively) Elastic modulus: 183.62±22.85 MPa and 210.29±19.20 MPa after post-heating >115°C for 300 s	[115]
PLA	Tn: 210°C Nozzle Ø: 400 µm Layer thickness: 200 µm Speed : 30 $mm.s^{-1}$ Pore size: 550-600 µm	Scaffold for bone regeneration	Pore size obtained (550 µm in XY and 620 µm in XZ) close to the designed pore size (650 µm in XY and 600 µm in XZ) thanks to FFF accuracy No significant degradation after 8 weeks in PBS at 37°C	[116]
PLA and PLA/5%HA	Tn: 200°C Nozzle Ø: 400 µm Layer thickness: 200 µm Speed: 50 $mm.s^{-1}$ Infill: 100% Perimeters: 3 Top/bottom layers: 3	Scaffold for bone TE	Successful fabrication of a porous 3D maxillary sinus via FFF Effects of HA: Good dispersion, ↑ flexural modulus (~7%) HA content should be increased	[117]

PLA and PLA/HA 50/50	Tn(first layer) : 190°C Tn(further layers) : 180°C Nozzle Ø : 900 µm Speed : 30 mm.s^{-1} Theoretical porosity: 50% Size: 12.7 × 12.7 × 25.4 mm^3	Scaffold for bone regeneration	FFF enables the use of particles, even in high amounts Effects of HA: ↑ surface roughness, homogeneous dispersion, ↑ porosity (from 39% to 55%), ↑ available surface area, amorphous material, ↓ stiffness (239 MPa to 124 MPa) but still compatible with that of trabecular bone (129 MPa)	[58]
PLA and PLA/15%HA	Tn(PLA): 180°C Tn(PLA/HA): 210°C Nozzle Ø: 350 µm Layer thickness: 200 µm Speed: 30 mm.s^{-1} Pore size: 700 µm (design 800 µm) + interconnectivity Porosity: 30%	Self-fitting implants for bone replacement	Obtained pore size of 700 µm close to that of the modeled pore size of 800 µm thanks to FFF Effect of HA: crack inhibition during compression-heating-compression cycles	[118]
PLA and PLA/Titanium (Ti) particles	Tn: 210°C Tp: 90°C Nozzle Ø: 400 µm Layer thickness: 200 µm Speed: 30 mm.s^{-1} Pore size: 560-790 µm Porosity: 47%	Scaffold for bone TE	FFF permitted to obtain a porous scaffold with controlled porosity and without cracks or defects, matching the initial design ↑ compressive/tensile properties with 5 vol% and 10 vol% of Ti Compressive strengths and moduli in the ranges of 20–30 MPa and 5–7 GPa (between those of human cancellous and cortical bones) Improved biocompatibility with Ti particles Higher surface roughness with Ti (↑ cell attachment + osteogenic differentiation)	[119]
PLGA-based scaffolds				
PLGA; comparison with PCL	Tn: 110°C Pressure: 670 kPa Nozzle Ø: 350 µm No chamber = fabrication at room temperature Size: 10 × 10 × 5 mm^3 Pore size: 600 µm + interconnectivity	Scaffold for bone TE	FFF was found to be a promising tool for scaffold fabrication (uniform pore size, regular layers throughout the scaffold thickness) Compressive modulus: 2.55 ± 0.11 MPa PLGA = safe scaffold material Bone generation but high degradation (no scaffold structure remained) PCL was judged more promising (longer degradation rate = better for large defects) even without carrying cells before insertion	[111]
PLGA and PLGA/collagen II	Tn: 170°C Nozzle Ø: 150 µm Cylinder: Ø 7.5 mm; height 2.5 mm Stacking angles in 4D (0°/90°/45°/135°) or 8D	Scaffolds for cartilage TE	FFF induced a decrease of PLGA M_w of 40% PLGA scaffolds: interconnected macropores PLGA/collagen II scaffolds: sponge-like structure (50–150 µm pores +	[107]

	(0°/90°/45°/135°/22.5°/67.5°/ 112.5°/157.5°) Spacing between adjacent fibers in the same layer: 0.35 mm, 0.65 mm or 1.15 mm		interconnectivity) Mechanical strength comparable to that of native cartilage ↑ cell seeding ratio from 70% to 90% for higher fiber spacing Smaller fiber spacing induced accumulation of acidic degradation products = autocatalytic effect and further degradation	
PCL-based scaffolds				
PCL	Tn: 80°C-90°C Nozzle Ø: 400 µm Speed: 5 $mm.s^{-1}$ Number of layers: 4	Scaffolds for TE	The FFF technology used did not strongly affect the geometry of the samples Complete cell (fibroblasts) adhesion and colonization of the structure	[120]
PCL and PCL/β-TCP; comparison with collagen	Tn: 110°C Pressure: 500 kPa Line width: 500 µm Size: 10 × 10 × 0.32 mm^3 Pore size: 250 µm	Membrane for guided bone regeneration (dentistry)	FFF permitted the use of biomaterials, blends and addition of powders + greater structural stability than that of commercially available collagen membranes Higher mechanical properties of collagen when dry Higher elastic modulus of PCL (171 MPa) and PCL/β-TCP (213 MPa) when wet (collagen: 12 MPa) Similar tensile stresses when wet: ~ 5 MPa PCL/β-TCP membrane demonstrated better bone regeneration performance than the collagen membrane	[52]
PCL + chitosan hydrogel filling (hybrid scaffold)	Tn:130°C Pressure: 1.5-3.0 bar Nozzle Ø: 400 µm Speed: 1-3 $mm.s^{-1}$ Pore size: 325.2 ± 26.3 µm Porosity: 62.4 ± 0.23%	Scaffold for bone TE	FFF allowed the printing of a porous PCL scaffold with well-controlled open and interconnected pores that allowed for a successful hydrogel filling afterwards Compressive strength: 6.7 MPa Low degradation ratio of PCL Favorable microenvironment for cell growth and osteogenesis	[121]
PCL and PCL/HA15%	Lay-down pattern: 0°/60°/120° Size: 10 × 10 × 8 mm Porosity: 65%	Scaffold for bone TE	FFF-made scaffolds may have a load-bearing application compared to foams that have low strength and low stiffness Stiffness: 7-11 MPa Increased after *in vivo* implantation = growth of tissue and ECM Constant rate of cell proliferation Tissue sheets were observed No significant difference between PCL and PCL/HA	[122]

475

Several benefits of FFF for the production of scaffolds can be identified from all of these studies; the main one being the fine control of the scaffold structure. The differences between the modeled scaffolds and the printed ones reside in the polymer thermal expansion during printing or shrinkage but this can be rectified by designing slightly wider pores, knowing the polymer thermal behavior, or readjusting the printing parameters. Also, it has been highlighted that the structures of the scaffolds obtained by FFF are more likely to enable load-bearing, as compared to traditional techniques that often lead to scaffolds with low strength and stiffness [122]. Moreover, the ability to use a variety of materials, even those composed of particles, offers promising new possibilities. Therefore, a well-set FFF process combined to a good choice of materials and bioactivity "boosters" provide very promising perspectives for scaffolding in TE.

However, further disadvantages of the FFF technique also emerge from these studies. Material degradation can occur at high temperature, when hydrolysis-sensitive polymers are processed, which is most often the case, but this problem can be partially solved, by thoroughly drying the materials before printing. In addition, low-temperature deposition manufacturing techniques based on FFF can be used [123]. The main drawback that can be deduced by looking at Table 2 is the limited resolution conditioned by the nozzle diameter. Indeed, the smallest nozzle diameter of all the studies described was found to be 150 µm. This results in a deposited filament with a thickness equal to or greater than this value and, therefore, scaffolds with rather low porosities (30% to 65%) compared to what can be obtained with other techniques (e.g. porosity of 94% with electrospinning [124]). In addition, the use of small diameter nozzles limits the ability to process materials that contain particles or fibers as they can cause clogging.

Nevertheless, the FFF process offers many new possibilities, among which the use of shape-memory polymers for scaffolding seems to be of particular interest.

IV. Shape-memory polymers for scaffolding

IV.1. Principle of SMPs for biomedical applications

Shape-memory polymers (SMPs) are of great interest in biomedical applications based on the principle that a small temporary shape can be used to avoid invasive surgery and facilitate patients' healing (Figure 8).

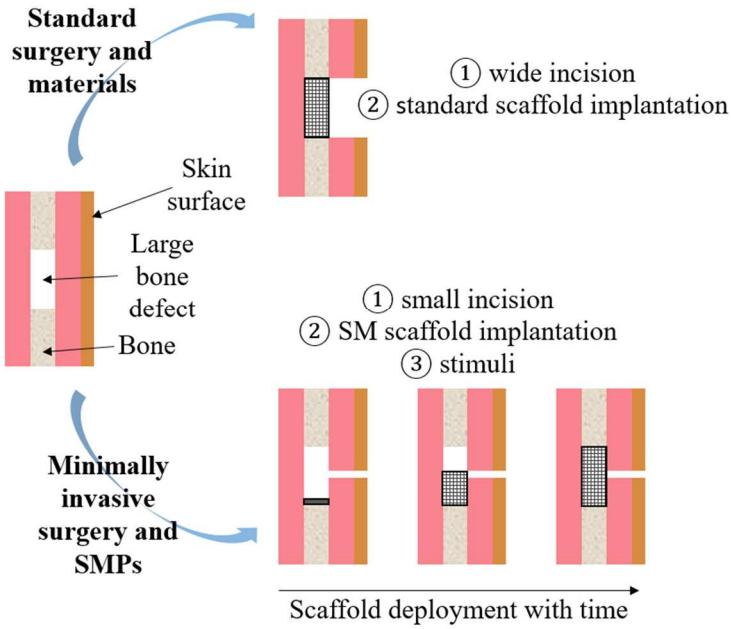

Figure 8 : Example of the interest of using SMPs for minimally invasive scaffold implantation for large bone defects

SMPs can recover from a temporary shape to their permanent shape under certain external stimuli, such as water [125], pH [126], light/laser [127–129], magnetism [130] or temperature [131,132]. Most reported SMPs are thermo-activated and have two different phases, a hard phase and a switching phase [133]. They can be deformed from their permanent shape (Figure 9 a) to a temporary shape by increasing temperature above their transition temperature (T_{trans}) (Figure 9 b) and by applying a certain strain (Figure 9 c) to respectively soften and deform the switching segments (reversible). The temporary shape is then fixed by decreasing temperature below T_{trans} and maintaining the strain (Figure 9 d). By re-increasing temperature above T_{trans}, the deformed part recovers its permanent shape through the hard segments (Figure 9 e).

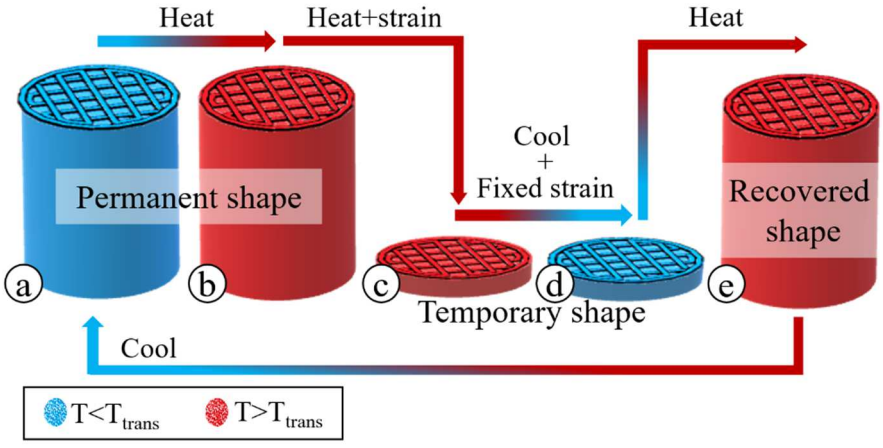

Figure 9 : Mechanism of a thermo-sensitive SMP scaffold

519 T_{trans} is generally a melting temperature (T_m) or a T_g, depending on the polymer type
520 (thermoset, thermoplastic, blend, copolymer, amorphous or semi-crystalline polymer) and on
521 the type of cross-links. Cross-links can be chemical (covalent bonds) and physical (weak
522 interactions, crystalline domains, entanglements, etc.), and enable to set the permanent shape
523 and to return to it upon heating above T_{trans} while the switching segments are soft [134].

524 The ability of an SMP to recover its permanent shape can be quantified by the shape-recovery
525 ratio (R_r) according to equation (1).

$$R_r = \frac{\varepsilon_u - \varepsilon_{p(N)}}{\varepsilon_m - \varepsilon_{p(N-1)}} \times 100 \quad (1)$$

526 Where N is the cycle number, ε_p is the strain of the stress-free sample before applying yield
527 stress. ε_u is the strain of the stress-free sample after the programming step and ε_m is the
528 maximum strain under loading [135]. The higher the R_r, the more complete the recovery of
529 the part.

530 Shape-fixity ratio (R_f), on the other hand, characterizes the material's ability to keep its given
531 temporary shape. It can be calculated by following equation (2) [135].

$$R_f = \frac{\varepsilon_{u(N)}}{\varepsilon_m} \times 100 \quad (2)$$

532 Achieving a high R_f is essential to prevent the part from premature expansion and recoil
533 [136]. Figure 10 represents these notions. After heating (1), the polymer is loaded (2) and
534 cooled down under loading (3). Then, the scaffold is unloaded (4) and goes from its maximum
535 strain under compression (ε_m) to its strain without stress (ε_u), and it can be noticed in this
536 example that shape fixity is not equal to 100% as $\varepsilon_m \neq \varepsilon_u$. After being reheated (5), the
537 scaffold recovers its permanent shape but does not reach a 0% strain, revealing that shape
538 recovery is not optimal either.

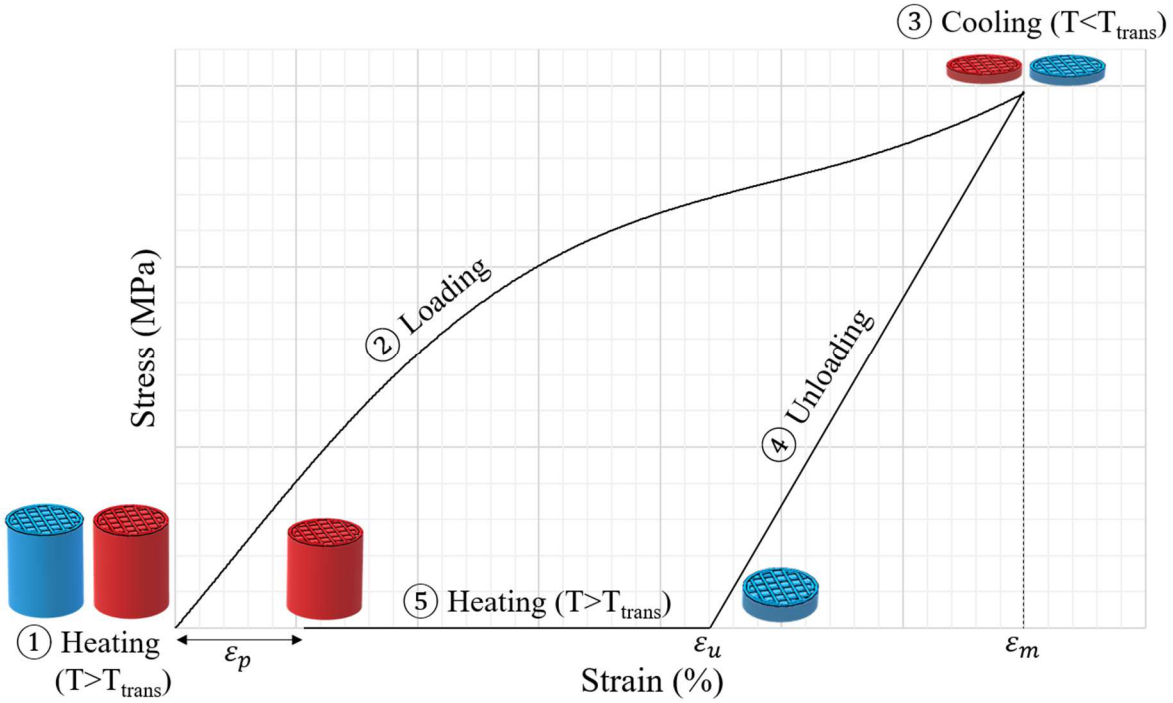

Figure 10 : Shape memory cycle test on an SMP scaffold

Various chemical and physical networks can trigger shape-fixing and shape-recovery mechanisms, dividing SMPs in several different categories. Liu *et al.* classify them in four categories: chemically cross-linked glassy thermosets, chemically cross-linked semi-crystalline rubbers, physically cross-linked thermoplastics and physically cross-linked block copolymers [137]. Other classifications also exist. Sun *et al.* classified SMPs into two categories: covalently/physically cross-linked polymer network structures and polymer blends [138]. Indeed, blending two immiscible polymers together permits to generate two immiscible phases, with one of the polymers being highly crystalline and acting as the hard phase while the other one is amorphous and acts as the switching phase. Karger-Kocsis and Kéki distinguish thermo-activated SMPs as a function of their T_{trans}, which is either a T_g or a T_m [139].

SMPs are used in biomedical applications based on the facts that the body has a temperature of 37°C (for heat-activated SMPs), that its pH is about 7.4 (for pH-activated SMPs) and that it contains water (for water-activated SMPs). Sometimes, SMPs with several stimuli can be obtained, such as in the study of Sessini *et al.*, who designed blends of ethylene-vinyl acetate and thermoplastic starch responsive to both humidity and thermal stimuli [140].

IV.2. Biodegradable and biocompatible SMPs

PUs include thermosetting PUs and thermoplastic PUs, also known as TPUs. The latter are copolymers with alternating hard and soft segments. Depending on the nature of these segments, their proportion, etc., an impressive variety of TPUs can be synthesized with all kinds of properties, such as shape memory (SM) for some of them. Biodegradable PU-based SMPs seem to have potential for medical applications because of their properties such as their biocompatibility and their T_g that can be tailored [141]. PCL, PLLA, PLGA, and many others, can be used as soft segments [142]. However, elasticity is not always optimal and the rate of biodegradation of such PU-based SMPs is lower (weight loss < 2.5% after 10 weeks of immersion in PBS at 37°C) than that of other common biodegradable polymers (weight loss close to 65% after 10 weeks for PLGA in the same conditions [63]). Blends of TPU and other polymers such as PLA are commonly used to enhance the degradation rate of the resulting material and as a counterpart, increase the other polymer SM properties [143,144]. Many other biodegradable polymers (PLA, PCL etc.) present SM properties. However, the main problems are that the recovery stress, shape-recovery, shape-fixity ratios, etc. may not be high enough to be used for very precise applications such as in the biomedical field. Moreover, PLA is brittle, poorly resistant to impact and has a low elongation at break, reducing its suitability as SMP with high strain ratios. For these reasons, polymers are rarely used pure, but rather blended with other matrices, additives and/or plasticizers. Custom copolymers can also be synthesized to meet specific needs. In Zheng *et al.*'s research, the addition of particles (HA) improved the shape-memory effect (SME) of PDLLA composites, which exhibited higher shape-recovery ratios (over 95%) as well as faster recovery times (higher speeds of recovery) as compared to pure PDLLA (R_r around 80%) [145]. Zhang *et al.* managed to enhance PLA elongation at break by blending it with biodegradable polyamide elastomer, while providing it with remarkable SM properties (recovery to permanent shape after 100% strain in 8 s and 3 s at 80°C and 90°C, respectively) [146]. However, in order to be used in the biomedical field, the T_{trans} of SMPs should be lower than 60°C and this temperature should only be maintained for a short period of time to avoid tissue necrosis [147]. The use of plasticizers can be a good way to decrease the T_{trans} of SMPs by enhancing chain mobility, while increasing the elongation at break of fragile polymers such as PLA. Poly (ethylene glycol) (PEG) is often used because of its biocompatibility and has been found in numerous studies, blended (or copolymerized) with PLA and other polymers [148–151]. Cai *et al.* were able to decrease the T_{trans} of PLA/TPU blends and noticed a threshold value (10% PEG) above

which the increase in SM properties was no longer significant [150]. In the study of Guo *et al.*, PEG blended with PLA permitted to obtain suitable morphology (fewer pores, as samples were produced by solvent evaporation), hydrophilicity, and mechanical properties without too much impacting the SM properties [149]. Peterson *et al.* published a complete review dedicated to biodegradable SMPs in medicine, where a table containing 50 different formulations can be found [152].

IV.3. 4D printing for scaffold production via FFF

4D polymer printing combines the advantages of AM and those of SMPs to make smart objects. With time as an additional dimension to 3D printing, the term 4D printing was introduced. An example of a 4D printed object is given in Figure 11. A heart-shaped part was 4D printed via FFF and placed in hot water (~70°C) to be deformed into a temporary shape (Figure 11-0 s) by holding the part during cooling. The temporary shape was then placed in a hot water bath at 70°C and its recovery was recorded until the part regained its permanent shape (Figure 11-1 min 30 s).

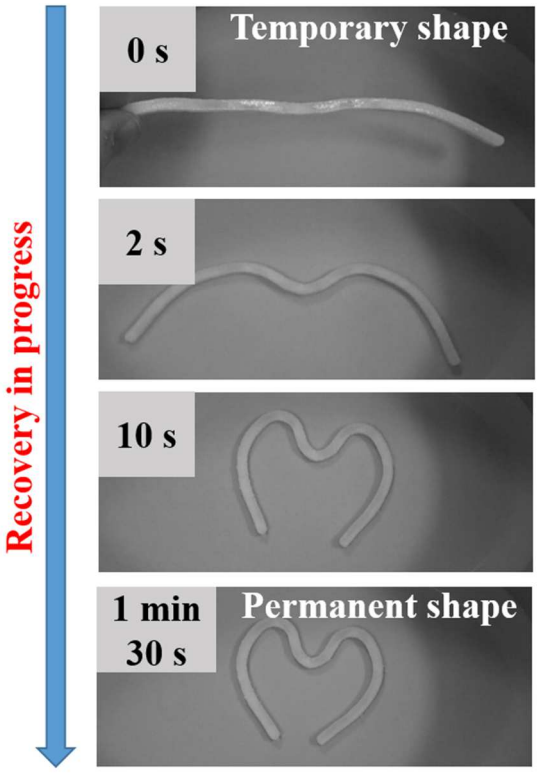

Figure 11 : 4D printed heart-shaped object taking back its permanent shape from a temporary shape (0 s) in hot water ~70°C; TPU with a T_{trans} of 43°C

As mentioned earlier, not all thermoplastics are easily printable via FFF and are well suited to biomedical applications and many fewer have SM properties. Therefore, only a few 4D printed (FFF) scaffolds were found in the literature. Senatov *et al.* used PLA to manufacture SM porous scaffolds (Figure 12 and Figure 13) because of its suitable rheological and SM properties, due to physical entanglements of the long chains of PLA, playing the role of fixing phase [118,153].

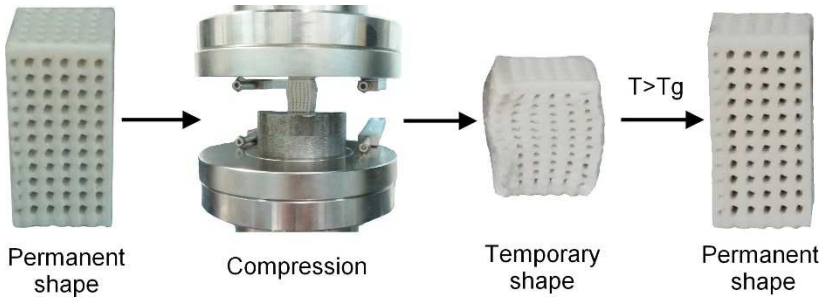

Figure 12 : 4D printed scaffold programming and recovery. Reprinted with permission from Ref. [118], copyright (2016), Elsevier.

They added inorganic particles of high stiffness, in this particular case, HA, to provide bioactivity as well as an additional fixing phase. In their first study, they almost doubled the compression strength (at 15% strain) of the HA-filled scaffold as compared to that of the pure PLA one and achieved a great shape-recovery ratio of 98% after the first compression cycle [118]. They also reached a maximum recovery stress of 3 MPa at 70°C but concluded that the SME activation temperature should be decreased for their scaffolds to be deployed in the human body. In the second study, they revealed that their PLA/HA SM scaffolds induced viable MSCs and stimulated their proliferation [153].

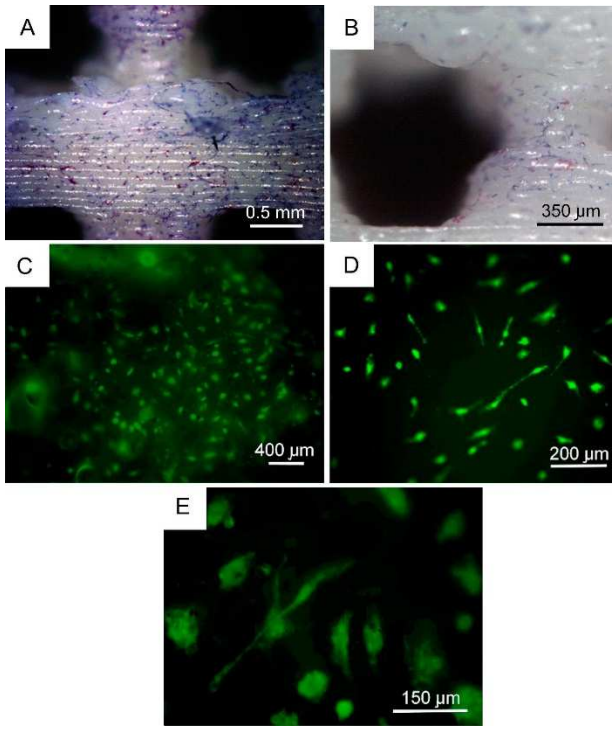

Figure 13 : PLA/HA 4D printed (FFF) scaffold showing, in green, MSC colonization at its surface. Reprinted with permission from Ref. [153], copyright (2017), Elsevier.

Kutikov *et al.* studied the SM properties of thermoplastic amphiphilic poly (D,L-lactic acid-*co*-ethylene glycol-*co*-D,L-lactic acid) (PELA) and HA-PELA composites and successfully printed (via FFF) biodegradable scaffolds from these materials, which exhibited rapid recovery (~3 s) at 50°C [147]. The SME of amphiphilic polymers can be attributed to segregation between the hydrophilic and hydrophobic phases, where the phase with the highest thermal transition induces the hard segments while the other phase constitutes the soft part. Hendrikson *et al.* used a shape-memory PU DiAPLEX® MM 3520 from SMP Technologies Inc. to print scaffolds and found maximum recovery at 37°C after 30 min [154]. They tried two raster orientations, 0°/45°/90° and 0°/90°/180° and revealed that the scaffolds built with the 0°/45°/90° raster orientation exhibited a higher shape recovery. As the surface of the scaffolds was not adequate for cell attachment, they functionalized them by covalently binding type I collagen. Results of MSC culture at 37°C for 14 days revealed 100% cell viability, leading to the conclusion that these scaffolds have potential to be used for tissue regeneration. However, the scaffold biodegradability was not assessed.

4D printing of scaffolds via FFF encounters similar difficulties as 3D printing via the same printing technique (limited mechanical properties, anisotropy, shrinkage/warpage of the parts, thermal degradation, rather low scaffold porosity, impossibility to use polymers other than thermoplastics). In 4D printing by FFF, these difficulties are more apparent as the choice of

materials is even more limited, particularly for the production of scaffolds. Indeed, these materials must be biocompatible, biodegradable, possess SM properties (with 37°C < T_{trans} << 60°C), in addition to being thermoplastic. These materials are rare, as evidenced by the scarcity of studies on the subject, and the development of new polymers meeting these criteria is growing.

Conclusions and perspectives

Additive manufacturing and especially fused filament fabrication (FFF) have a great future for medical applications, and affordable implants adapted to the patients' needs should become more common in the biomedical and regenerative medicine fields.

Many advantages of the FFF processing technique were highlighted in the reviewed studies, such as the possibility of printing complex load-bearing parts like scaffolds for tissue engineering (TE). Studies revealed the possibility of finely controlling the properties of the scaffolds (biocompatibility, bioactivity, biodegradation, mechanical properties, shape memory, etc.) by choosing appropriate materials (neat polymers, filled polymers, copolymers, polymer blends, etc.) and suitable scaffold structures (depending on process parameters like raster width, air gap, layer thickness, angle deposition, etc.). On the one hand, results described in this review are very promising and tend to encourage researchers to continue to optimize FFF printed scaffolds. On the other hand, a severe lack of available biomaterials well suited for scaffolding and developed especially for FFF was pointed out, opening up new research opportunities.

Moreover, many studies deal with the influence of printing parameters on the properties of the parts but these studies generally use materials that are not adapted for scaffolding. Research also seems to be at an academic level since the printed parts are often test specimens and not parts for special applications. This induces many research perspectives in the field of scaffolds for TE produced by FFF, since printing parameters have an influence on their properties. This has been addressed in a few studies but this has rarely been combined with shape-memory polymers (SMPs), even though printing parameters seem to have a great effect on their efficient deployment in the human body. Nevertheless, the few studies concerning 4D printing for the production of scaffolds are very encouraging and make the use of SMPs realistic for this kind of application.

Declaration of interest

The authors declare that they have no known competing financial interests or personal relationships that could have appeared to influence the work reported in this paper.

Acknowledgements

The authors acknowledge the Interreg France-Wallonie-Vlaanderen program, 3D4Med, with the financial support of the European Regional Development Fund (ERDF). The authors would also like to address special thanks to Dr. Halima Kerdjoudj for her help and advice.

References

[1] A. Standard, ISO/ASTM 52900: 2015 Additive manufacturing-General principles-terminology, ASTM F2792-10e1. (2012).

[2] Q. Yan, H. Dong, J. Su, J. Han, B. Song, Q. Wei, Y. Shi, A Review of 3D Printing Technology for Medical Applications, Engineering. 4 (2018) 729–742. https://doi.org/10.1016/j.eng.2018.07.021.

[3] R. Huiskes, R. Ruimerman, G.H. van Lenthe, J.D. Janssen, Effects of mechanical forces on maintenance and adaptation of form in trabecular bone, Nature. 405 (2000) 704–706. https://doi.org/10.1038/35015116.

[4] H. Cao, N. Kuboyama, A biodegradable porous composite scaffold of PGA/β-TCP for bone tissue engineering, Bone. 46 (2010) 386–395. https://doi.org/10.1016/j.bone.2009.09.031.

[5] M. Sadat-Shojai, M.-T. Khorasani, A. Jamshidi, S. Irani, Nano-hydroxyapatite reinforced polyhydroxybutyrate composites: A comprehensive study on the structural and in vitro biological properties, Mater. Sci. Eng. C. 33 (2013) 2776–2787. https://doi.org/10.1016/j.msec.2013.02.041.

[6] S.I. Jeong, E.K. Ko, J. Yum, C.H. Jung, Y.M. Lee, H. Shin, Nanofibrous Poly(lactic acid)/Hydroxyapatite Composite Scaffolds for Guided Tissue Regeneration, Macromol. Biosci. 8 (2008) 328–338. https://doi.org/10.1002/mabi.200700107.

[7] H. Ma, W. Su, Z. Tai, D. Sun, X. Yan, B. Liu, Q. Xue, Preparation and cytocompatibility of polylactic acid/hydroxyapatite/graphene oxide nanocomposite fibrous membrane, Chin. Sci. Bull. 57 (2012) 3051–3058. https://doi.org/10.1007/s11434-012-5336-3.

[8] K.G. Marra, J.W. Szem, P.N. Kumta, P.A. DiMilla, L.E. Weiss, In vitro analysis of biodegradable polymer blend/hydroxyapatite composites for bone tissue engineering, J. Biomed. Mater. Res. 47 (1999) 324–335. https://doi.org/10.1002/(SICI)1097-4636(19991205)47:3<324::AID-JBM6>3.0.CO;2-Y.

[9] L.M. Mathieu, T.L. Mueller, P.-E. Bourban, D.P. Pioletti, R. Müller, J.-A.E. Månson, Architecture and properties of anisotropic polymer composite scaffolds for bone tissue engineering, Biomaterials. 27 (2006) 905–916. https://doi.org/10.1016/j.biomaterials.2005.07.015.

[10] S. Singh, S. Ramakrishna, R. Singh, Material issues in additive manufacturing: A review, J. Manuf. Process. 25 (2017) 185–200. https://doi.org/10.1016/j.jmapro.2016.11.006.

716 [11] H. Bikas, P. Stavropoulos, G. Chryssolouris, Additive manufacturing methods and
717 modelling approaches: a critical review, Int. J. Adv. Manuf. Technol. 83 (2016) 389–
718 405. https://doi.org/10.1007/s00170-015-7576-2.
719 [12] C.-C. Kuo, L.-C. Liu, W.-F. Teng, H.-Y. Chang, F.-M. Chien, S.-J. Liao, W.-F. Kuo,
720 C.-M. Chen, Preparation of starch/acrylonitrile-butadiene-styrene copolymers (ABS)
721 biomass alloys and their feasible evaluation for 3D printing applications, Compos. Part
722 B Eng. 86 (2016) 36–39. https://doi.org/10.1016/j.compositesb.2015.10.005.
723 [13] L.M. Galantucci, F. Lavecchia, G. Percoco, Experimental study aiming to enhance the
724 surface finish of fused deposition modeled parts, CIRP Ann. 58 (2009) 189–192.
725 https://doi.org/10.1016/j.cirp.2009.03.071.
726 [14] C. Duty, C. Ajinjeru, V. Kishore, B. Compton, N. Hmeidat, X. Chen, P. Liu, A.A.
727 Hassen, J. Lindahl, V. Kunc, What makes a material printable? A viscoelastic model
728 for extrusion-based 3D printing of polymers, J. Manuf. Process. 35 (2018) 526–537.
729 https://doi.org/10.1016/j.jmapro.2018.08.008.
730 [15] P. Szymczyk-Ziółkowska, M.B. Łabowska, J. Detyna, I. Michalak, P. Gruber, A review
731 of fabrication polymer scaffolds for biomedical applications using additive
732 manufacturing techniques, Biocybern. Biomed. Eng. 40 (2020) 624–638.
733 https://doi.org/10.1016/j.bbe.2020.01.015.
734 [16] A. Gleadall, D. Visscher, J. Yang, D. Thomas, J. Segal, Review of additive
735 manufactured tissue engineering scaffolds: relationship between geometry and
736 performance, Burns Trauma. 6 (2018). https://doi.org/10.1186/s41038-018-0121-4.
737 [17] N. Poomathi, S. Singh, C. Prakash, A. Subramanian, R. Sahay, A. Cinappan, S.
738 Ramakrishna, 3D printing in tissue engineering: a state of the art review of
739 technologies and biomaterials, Rapid Prototyp. J. 26 (2020) 1313–1334.
740 https://doi.org/10.1108/RPJ-08-2018-0217.
741 [18] D.G. Tamay, T.D. Usal, A.S. Alagoz, D. Yucel, N. Hasirci, V. Hasirci, 3D and 4D
742 Printing of Polymers for Tissue Engineering Applications, Front. Bioeng. Biotechnol. 7
743 (2019).
744 [19] Y. Liu, W. Wang, L.-C. Zhang, Additive manufacturing techniques and their
745 biomedical applications, Fam. Med. Community Health. 5 (2017) 286–298.
746 https://doi.org/10.15212/FMCH.2017.0110.
747 [20] S. Gupta, A. Bissoyi, A. Bit, A review on 3D printable techniques for tissue
748 engineering, BioNanoScience. 8 (2018) 868–883.
749 [21] N. Sabahi, W. Chen, C.-H. Wang, J.J. Kruzic, X. Li, A Review on Additive
750 Manufacturing of Shape-Memory Materials for Biomedical Applications, JOM. 72
751 (2020) 1229–1253. https://doi.org/10.1007/s11837-020-04013-x.
752 [22] Y. Li, F. Zhang, Y. Liu, J. Leng, 4D printed shape memory polymers and their
753 structures for biomedical applications, Sci. China Technol. Sci. 63 (2020) 545–560.
754 https://doi.org/10.1007/s11431-019-1494-0.
755 [23] D.W. Hutmacher, Scaffolds in tissue engineering bone and cartilage, in: Biomater.
756 Silver Jubil. Compend., Elsevier, 2000: pp. 175–189.
757 [24] F.J. O'Brien, Biomaterials & scaffolds for tissue engineering, Mater. Today. 14 (2011)
758 88–95. https://doi.org/10.1016/S1369-7021(11)70058-X.
759 [25] L.E. Freed, G. Vunjak-Novakovic, R.J. Biron, D.B. Eagles, D.C. Lesnoy, S.K. Barlow,
760 R. Langer, Biodegradable polymer scaffolds for tissue engineering, Bio/Technology. 12
761 (1994) 689.
762 [26] B. Dhandayuthapani, Y. Yoshida, T. Maekawa, D.S. Kumar, Polymeric Scaffolds in
763 Tissue Engineering Application: A Review, Int. J. Polym. Sci. 2011 (2011) e290602.
764 https://doi.org/10.1155/2011/290602.

765 [27] K. Madhavan Nampoothiri, N.R. Nair, R.P. John, An overview of the recent
766 developments in polylactide (PLA) research, Bioresour. Technol. 101 (2010) 8493–
767 8501. https://doi.org/10.1016/j.biortech.2010.05.092.
768 [28] Y. Zhao, Z. Wang, J. Wang, H. Mai, B. Yan, F. Yang, Direct synthesis of poly(D,L-
769 lactic acid) by melt polycondensation and its application in drug delivery, J. Appl.
770 Polym. Sci. 91 (2004) 2143–2150. https://doi.org/10.1002/app.13354.
771 [29] P. Saini, M. Arora, M.N.V.R. Kumar, Poly(lactic acid) blends in biomedical
772 applications, Adv. Drug Deliv. Rev. 107 (2016) 47–59.
773 https://doi.org/10.1016/j.addr.2016.06.014.
774 [30] P. Alves, P. Ferreira, M.H. Gil, Biomedical polyurethane-based materials, Polyurethane
775 Prop. Struct. Appl. N. Y. Nova Publ. (2012) 1–25.
776 [31] W. Bonfield, M.D. Grynpas, A.E. Tully, J. Bowman, J. Abram, Hydroxyapatite
777 reinforced polyethylene–a mechanically compatible implant material for bone
778 replacement., Biomaterials. 2 (1981) 185–186.
779 [32] M. Wang, R. Joseph, W. Bonfield, Hydroxyapatite-polyethylene composites for bone
780 substitution: effects of ceramic particle size and morphology, Biomaterials. 19 (1998)
781 2357–2366. https://doi.org/10.1016/S0142-9612(98)00154-9.
782 [33] M. Hashimoto, H. Takadama, M. Mizuno, Y. Yasutomi, T. Kokubo, Titanium
783 dioxide/ultra high molecular weight polyethylene composite for bone-repairing
784 applications: preparation and biocompatibility, in: Key Eng. Mater., Trans Tech Publ,
785 2003: pp. 415–418.
786 [34] V.R. Sastri, Plastics in medical devices: properties, requirements, and applications,
787 William Andrew, 2013.
788 [35] H.M. Clayman, Polypropylene, Ophthalmology. 88 (1981) 959–964.
789 https://doi.org/10.1016/S0161-6420(81)80012-7.
790 [36] B. Hinsch, Surgical filament from polypropylene blended with polyethylene, 1985.
791 [37] L. Nässberger, A. Arbin, J. Östelius, Exposure of patients to phthalates from polyvinyl
792 chloride tubes and bags during dialysis, Nephron. 45 (1987) 286–290.
793 [38] B. Singh, L. Pal, Sterculia crosslinked PVA and PVA-poly(AAm) hydrogel wound
794 dressings for slow drug delivery: Mechanical, mucoadhesive, biocompatible and
795 permeability properties, J. Mech. Behav. Biomed. Mater. 9 (2012) 9–21.
796 https://doi.org/10.1016/j.jmbbm.2012.01.021.
797 [39] S. Kayal, R.V. Ramanujan, Doxorubicin loaded PVA coated iron oxide nanoparticles
798 for targeted drug delivery, Mater. Sci. Eng. C. 30 (2010) 484–490.
799 https://doi.org/10.1016/j.msec.2010.01.006.
800 [40] P.E. Feuser, P.C. Gaspar, E. Ricci-Júnior, M.C.S. da Silva, M. Nele, C. Sayer, P.H.H.
801 de Araújo, Synthesis and Characterization of Poly(Methyl Methacrylate) PMMA and
802 Evaluation of Cytotoxicity for Biomedical Application, Macromol. Symp. 343 (2014)
803 65–69. https://doi.org/10.1002/masy.201300194.
804 [41] P. Lopes, M. Corbellini, B.L. Ferreira, N. Almeida, M. Fredel, M.H. Fernandes, R.
805 Correia, New PMMA-co-EHA glass-filled composites for biomedical applications:
806 Mechanical properties and bioactivity, Acta Biomater. 5 (2009) 356–362.
807 https://doi.org/10.1016/j.actbio.2008.07.012.
808 [42] I.V. Panayotov, V. Orti, F. Cuisinier, J. Yachouh, Polyetheretherketone (PEEK) for
809 medical applications, J. Mater. Sci. Mater. Med. 27 (2016) 118.
810 https://doi.org/10.1007/s10856-016-5731-4.
811 [43] M. Vaezi, S. Yang, Extrusion-based additive manufacturing of PEEK for biomedical
812 applications, Virtual Phys. Prototyp. 10 (2015) 123–135.
813 https://doi.org/10.1080/17452759.2015.1097053.

[44] K.Y. Lee, D.J. Mooney, Alginate: Properties and biomedical applications, Prog. Polym. Sci. 37 (2012) 106–126. https://doi.org/10.1016/j.progpolymsci.2011.06.003.
[45] C. Meena, S.A. Mengi, S.G. Deshpande, Biomedical and industrial applications of collagen, Proc. Indian Acad. Sci. - Chem. Sci. 111 (1999) 319–329. https://doi.org/10.1007/BF02871912.
[46] C.H. Lee, A. Singla, Y. Lee, Biomedical applications of collagen, Int. J. Pharm. 221 (2001) 1–22. https://doi.org/10.1016/S0378-5173(01)00691-3.
[47] Y.-C. Lin, F. Tan, K.G. Marra, S.-S. Jan, D.-C. Liu, Synthesis and characterization of collagen/hyaluronan/chitosan composite sponges for potential biomedical applications, Acta Biomater. 5 (2009) 2591–2600. https://doi.org/10.1016/j.actbio.2009.03.038.
[48] W.K. Czaja, D.J. Young, M. Kawecki, R.M. Brown, The Future Prospects of Microbial Cellulose in Biomedical Applications, Biomacromolecules. 8 (2007) 1–12. https://doi.org/10.1021/bm060620d.
[49] M. Bernard, E. Jubeli, M.D. Pungente, N. Yagoubi, Biocompatibility of polymer-based biomaterials and medical devices – regulations, in vitro screening and risk-management, Biomater. Sci. 6 (2018) 2025–2053. https://doi.org/10.1039/C8BM00518D.
[50] T. Kumaresan, R. Gandhinathan, M. Ramu, M. Ananthasubramanian, K.B. Pradheepa, Design, analysis and fabrication of polyamide/hydroxyapatite porous structured scaffold using selective laser sintering method for bio-medical applications, J. Mech. Sci. Technol. 30 (2016) 5305–5312.
[51] C.X. Lam, S.H. Teoh, D.W. Hutmacher, Comparison of the degradation of polycaprolactone and polycaprolactone–(β-tricalcium phosphate) scaffolds in alkaline medium, Polym. Int. 56 (2007) 718–728. https://doi.org/10.1002/pi.2195.
[52] J.-H. Shim, J.-Y. Won, J.-H. Park, J.-H. Bae, G. Ahn, C.-H. Kim, D.-H. Lim, D.-W. Cho, W.-S. Yun, E.-B. Bae, C.-M. Jeong, J.-B. Huh, Effects of 3D-Printed Polycaprolactone/β-Tricalcium Phosphate Membranes on Guided Bone Regeneration, Int. J. Mol. Sci. 18 (2017) 899. https://doi.org/10.3390/ijms18050899.
[53] N. Tamai, A. Myoui, M. Hirao, T. Kaito, T. Ochi, J. Tanaka, K. Takaoka, H. Yoshikawa, A new biotechnology for articular cartilage repair: subchondral implantation of a composite of interconnected porous hydroxyapatite, synthetic polymer (PLA-PEG), and bone morphogenetic protein-2 (rhBMP-2), Osteoarthritis Cartilage. 13 (2005) 405–417. https://doi.org/10.1016/j.joca.2004.12.014.
[54] M. Wang, Bioactive Materials and Processing, in: D. Shi (Ed.), Biomater. Tissue Eng., Springer, Berlin, Heidelberg, 2004: pp. 1–82. https://doi.org/10.1007/978-3-662-06104-6_1.
[55] A. Bruyas, F. Lou, A.M. Stahl, M. Gardner, W. Maloney, S. Goodman, Y.P. Yang, Systematic characterization of 3D-printed PCL/β-TCP scaffolds for biomedical devices and bone tissue engineering: Influence of composition and porosity, J. Mater. Res. 33 (2018) 1948–1959. https://doi.org/10.1557/jmr.2018.112.
[56] H. Chaair, H. Labjar, O. Britel, Synthesis of β-tricalcium phosphate, Morphologie. 101 (2017) 120–124. https://doi.org/10.1016/j.morpho.2017.06.002.
[57] Y. Abe, Y. Okazaki, K. Hiasa, K. Yasuda, K. Nogami, W. Mizumachi, I. Hirata, Bioactive Surface Modification of Hydroxyapatite, BioMed Res. Int. 2013 (2013) e626452. https://doi.org/10.1155/2013/626452.
[58] C. Esposito Corcione, F. Gervaso, F. Scalera, S.K. Padmanabhan, M. Madaghiele, F. Montagna, A. Sannino, A. Licciulli, A. Maffezzoli, Highly loaded hydroxyapatite microsphere/ PLA porous scaffolds obtained by fused deposition modelling, Ceram. Int. 45 (2019) 2803–2810. https://doi.org/10.1016/j.ceramint.2018.07.297.

[59] J.J. Blaker, J.E. Gough, V. Maquet, I. Notingher, A.R. Boccaccini, In vitro evaluation of novel bioactive composites based on Bioglass®-filled polylactide foams for bone tissue engineering scaffolds, J. Biomed. Mater. Res. A. 67A (2003) 1401–1411. https://doi.org/10.1002/jbm.a.20055.
[60] T. Serra, M.A. Mateos-Timoneda, J.A. Planell, M. Navarro, 3D printed PLA-based scaffolds, Organogenesis. 9 (2013) 239–244. https://doi.org/10.4161/org.26048.
[61] T. Serra, J.A. Planell, M. Navarro, High-resolution PLA-based composite scaffolds via 3-D printing technology, Acta Biomater. 9 (2013) 5521–5530. https://doi.org/10.1016/j.actbio.2012.10.041.
[62] G. Altankov, Th. Groth, Reorganization of substratum-bound fibronectin on hydrophilic and hydrophobic materials is related to biocompatibility, J. Mater. Sci. Mater. Med. 5 (1994) 732–737. https://doi.org/10.1007/BF00120366.
[63] J. Zhang, S.-G. Yang, J.-X. Ding, Z.-M. Li, Tailor-made poly(L-lactide)/poly(lactide-co-glycolide)/hydroxyapatite composite scaffolds prepared via high-pressure compression molding/salt leaching, RSC Adv. 6 (2016) 47418–47426. https://doi.org/10.1039/C6RA06906A.
[64] C.-T. Kao, C.-C. Lin, Y.-W. Chen, C.-H. Yeh, H.-Y. Fang, M.-Y. Shie, Poly(dopamine) coating of 3D printed poly(lactic acid) scaffolds for bone tissue engineering, Mater. Sci. Eng. C. 56 (2015) 165–173. https://doi.org/10.1016/j.msec.2015.06.028.
[65] M. Wang, P. Favi, X. Cheng, N.H. Golshan, K.S. Ziemer, M. Keidar, T.J. Webster, Cold atmospheric plasma (CAP) surface nanomodified 3D printed polylactic acid (PLA) scaffolds for bone regeneration, Acta Biomater. 46 (2016) 256–265. https://doi.org/10.1016/j.actbio.2016.09.030.
[66] B. Tyler, D. Gullotti, A. Mangraviti, T. Utsuki, H. Brem, Polylactic acid (PLA) controlled delivery carriers for biomedical applications, Adv. Drug Deliv. Rev. 107 (2016) 163–175. https://doi.org/10.1016/j.addr.2016.06.018.
[67] S. Toosi, H. Naderi-Meshkin, F. Kalalinia, M.T. Peivandi, H. HosseinKhani, A.R. Bahrami, A. Heirani-Tabasi, M. Mirahmadi, J. Behravan, PGA-incorporated collagen: Toward a biodegradable composite scaffold for bone-tissue engineering, J. Biomed. Mater. Res. A. 104 (2016) 2020–2028. https://doi.org/10.1002/jbm.a.35736.
[68] S.A. Park, S.H. Lee, W.D. Kim, Fabrication of porous polycaprolactone/hydroxyapatite (PCL/HA) blend scaffolds using a 3D plotting system for bone tissue engineering, Bioprocess Biosyst. Eng. 34 (2011) 505–513. https://doi.org/10.1007/s00449-010-0499-2.
[69] J.G. Speight, Chapter 14 - Monomers, Polymers, and Plastics, in: J.G. Speight (Ed.), Handb. Ind. Hydrocarb. Process., Gulf Professional Publishing, Boston, 2011: pp. 499–537. https://doi.org/10.1016/B978-0-7506-8632-7.10014-3.
[70] D. da Silva, M. Kaduri, M. Poley, O. Adir, N. Krinsky, J. Shainsky-Roitman, A. Schroeder, Biocompatibility, biodegradation and excretion of polylactic acid (PLA) in medical implants and theranostic systems, Chem. Eng. J. 340 (2018) 9–14. https://doi.org/10.1016/j.cej.2018.01.010.
[71] B.D. Ulery, L.S. Nair, C.T. Laurencin, Biomedical applications of biodegradable polymers, J. Polym. Sci. Part B Polym. Phys. 49 (2011) 832–864. https://doi.org/10.1002/polb.22259.
[72] C.-C. Chen, J.-Y. Chueh, H. Tseng, H.-M. Huang, S.-Y. Lee, Preparation and characterization of biodegradable PLA polymeric blends, Biomaterials. 24 (2003) 1167–1173. https://doi.org/10.1016/S0142-9612(02)00466-0.

[73] L. Wu, J. Ding, In vitro degradation of three-dimensional porous poly(d,l-lactide-co-glycolide) scaffolds for tissue engineering, Biomaterials. 25 (2004) 5821–5830. https://doi.org/10.1016/j.biomaterials.2004.01.038.
[74] C. Peng, J. Zheng, D. Chen, X. Zhang, L. Deng, Z. Chen, L. Wu, Response of hPDLSCs on 3D printed PCL/PLGA composite scaffolds in vitro, Mol. Med. Rep. 18 (2018) 1335–1344. https://doi.org/10.3892/mmr.2018.9076.
[75] J.P. Santerre, K. Woodhouse, G. Laroche, R.S. Labow, Understanding the biodegradation of polyurethanes: From classical implants to tissue engineering materials, Biomaterials. 26 (2005) 7457–7470. https://doi.org/10.1016/j.biomaterials.2005.05.079.
[76] L.A. Bosworth, S. Downes, Physicochemical characterisation of degrading polycaprolactone scaffolds, Polym. Degrad. Stab. 95 (2010) 2269–2276. https://doi.org/10.1016/j.polymdegradstab.2010.09.007.
[77] A. Garg, A. Bhattacharya, A. Batish, On Surface Finish and Dimensional Accuracy of FDM Parts after Cold Vapor Treatment, Mater. Manuf. Process. 31 (2016) 522–529. https://doi.org/10.1080/10426914.2015.1070425.
[78] D. Drummer, S. Cifuentes-Cuéllar, D. Rietzel, Suitability of PLA/TCP for fused deposition modeling, Rapid Prototyp. J. 18 (2012) 500–507.
[79] D. Vaes, M. Coppens, B. Goderis, W. Zoetelief, P. Van Puyvelde, Assessment of Crystallinity Development during Fused Filament Fabrication through Fast Scanning Chip Calorimetry, Appl. Sci. 9 (2019) 2676. https://doi.org/10.3390/app9132676.
[80] W.Z. Wu, P. Geng, J. Zhao, Y. Zhang, D.W. Rosen, H.B. Zhang, Manufacture and thermal deformation analysis of semicrystalline polymer polyether ether ketone by 3D printing, Mater. Res. Innov. 18 (2014) S5-12-S5-16. https://doi.org/10.1179/1432891714Z.000000000898.
[81] M. Spoerk, F. Arbeiter, I. Raguž, G. Weingrill, T. Fischinger, G. Traxler, S. Schuschnigg, L. Cardon, C. Holzer, Polypropylene Filled With Glass Spheres in Extrusion-Based Additive Manufacturing: Effect of Filler Size and Printing Chamber Temperature, Macromol. Mater. Eng. 303 (2018) 1800179. https://doi.org/10.1002/mame.201800179.
[82] T.-M. Wang, J.-T. Xi, Y. Jin, A model research for prototype warp deformation in the FDM process, Int. J. Adv. Manuf. Technol. 33 (2007) 1087–1096. https://doi.org/10.1007/s00170-006-0556-9.
[83] C. Bellehumeur, L. Li, Q. Sun, P. Gu, Modeling of Bond Formation Between Polymer Filaments in the Fused Deposition Modeling Process, J. Manuf. Process. 6 (2004) 170–178. https://doi.org/10.1016/S1526-6125(04)70071-7.
[84] C. Casavola, A. Cazzato, D. Karalekas, V. Moramarco, G. Pappalettera, The Effect of Chamber Temperature on Residual Stresses of FDM Parts, in: A. Baldi, S. Quinn, X. Balandraud, J.M. Dulieu-Barton, S. Bossuyt (Eds.), Residual Stress Thermomechanics Infrared Imaging Hybrid Tech. Inverse Probl. Vol. 7, Springer International Publishing, Cham, 2019: pp. 87–92. https://doi.org/10.1007/978-3-319-95074-7_16.
[85] M. Spoerk, J. Sapkota, G. Weingrill, T. Fischinger, F. Arbeiter, C. Holzer, Shrinkage and Warpage Optimization of Expanded-Perlite-Filled Polypropylene Composites in Extrusion-Based Additive Manufacturing, Macromol. Mater. Eng. 302 (2017) 1700143. https://doi.org/10.1002/mame.201700143.
[86] S.H. Kochesfahani, Improving PLA-based material for FDM 3D-printers using minerals (principles and method development), SPE ANTEC Indianap. (2016) 1598–1614.

[87] A. Boschetto, V. Giordano, F. Veniali, Modelling micro geometrical profiles in fused deposition process, Int. J. Adv. Manuf. Technol. 61 (2012) 945–956. https://doi.org/10.1007/s00170-011-3744-1.
[88] A. Boschetto, V. Giordano, F. Veniali, Surface roughness prediction in fused deposition modelling by neural networks, Int. J. Adv. Manuf. Technol. 67 (2013) 2727–2742. https://doi.org/10.1007/s00170-012-4687-x.
[89] D. Chaidas, K. Kitsakis, J. Kechagias, S. Maropoulos, The impact of temperature changing on surface roughness of FFF process, IOP Conf. Ser. Mater. Sci. Eng. 161 (2016) 012033. https://doi.org/10.1088/1757-899X/161/1/012033.
[90] P. Wang, B. Zou, S. Ding, Modeling of surface roughness based on heat transfer considering diffusion among deposition filaments for FDM 3D printing heat-resistant resin, Appl. Therm. Eng. 161 (2019) 114064.
[91] J.M. Chacón, M.A. Caminero, E. García-Plaza, P.J. Núñez, Additive manufacturing of PLA structures using fused deposition modelling: Effect of process parameters on mechanical properties and their optimal selection, Mater. Des. 124 (2017) 143–157. https://doi.org/10.1016/j.matdes.2017.03.065.
[92] A. Rodríguez-Panes, J. Claver, A.M. Camacho, The Influence of Manufacturing Parameters on the Mechanical Behaviour of PLA and ABS Pieces Manufactured by FDM: A Comparative Analysis, Materials. 11 (2018) 1333. https://doi.org/10.3390/ma11081333.
[93] D. Popescu, A. Zapciu, C. Amza, F. Baciu, R. Marinescu, FDM process parameters influence over the mechanical properties of polymer specimens: A review, Polym. Test. 69 (2018) 157–166. https://doi.org/10.1016/j.polymertesting.2018.05.020.
[94] M. Faes, E. Ferraris, D. Moens, Influence of inter-layer cooling time on the quasi-static properties of ABS components produced via fused deposition modelling, Procedia CIRP. 42 (2016) 748–753.
[95] T.E. Shelton, Z.A. Willburn, C.R. Hartsfield, G.R. Cobb, J.T. Cerri, R.A. Kemnitz, Effects of thermal process parameters on mechanical interlayer strength for additively manufactured Ultem 9085, Polym. Test. 81 (2020) 106255. https://doi.org/10.1016/j.polymertesting.2019.106255.
[96] S. Garzon-Hernandez, D. Garcia-Gonzalez, A. Jérusalem, A. Arias, Design of FDM 3D printed polymers: An experimental-modelling methodology for the prediction of mechanical properties, Mater. Des. 188 (2020) 108414. https://doi.org/10.1016/j.matdes.2019.108414.
[97] O.A. Mohamed, S.H. Masood, J.L. Bhowmik, Optimization of fused deposition modeling process parameters: a review of current research and future prospects, Adv. Manuf. 3 (2015) 42–53. https://doi.org/10.1007/s40436-014-0097-7.
[98] S. Singh, G. Singh, C. Prakash, S. Ramakrishna, Current status and future directions of fused filament fabrication, J. Manuf. Process. 55 (2020) 288–306. https://doi.org/10.1016/j.jmapro.2020.04.049.
[99] J. Xiao, Y. Gao, The manufacture of 3D printing of medical grade TPU, Prog. Addit. Manuf. 2 (2017) 117–123. https://doi.org/10.1007/s40964-017-0023-1.
[100] R. Bernasconi, G. Natale, M. Levi, L. Magagnin, Electroless plating of PLA and PETG for 3D printed flexible substrates, ECS Trans. 66 (2015) 23–35.
[101] R. Chen, A. Ramachandran, C. Liu, F.-K. Chang, D. Senesky, Tsai-Wu Analysis of a Thin-Walled 3D-Printed Polylactic Acid (PLA) Structural Bracket, in: 58th AIAAASCEAHSASC Struct. Struct. Dyn. Mater. Conf., American Institute of Aeronautics and Astronautics, n.d. https://doi.org/10.2514/6.2017-0567.
[102] B.B. Shahriar, C. France, N. Valerie, C. Arthur, G. Christian, Toward improvement of the properties of parts manufactured by FFF (fused filament fabrication) through

understanding the influence of temperature and rheological behaviour on the coalescence phenomenon, in: AIP Conf. Proc., AIP Publishing LLC, 2017: p. 040008.
[103] M. Heidari-Rarani, M. Rafiee-Afarani, A.M. Zahedi, Mechanical characterization of FDM 3D printing of continuous carbon fiber reinforced PLA composites, Compos. Part B Eng. 175 (2019) 107147. https://doi.org/10.1016/j.compositesb.2019.107147.
[104] M. Grasso, L. Azzouz, P. Ruiz-Hincapie, M. Zarrelli, G. Ren, Effect of temperature on the mechanical properties of 3D-printed PLA tensile specimens, Rapid Prototyp. J. 24 (2018) 1337–1346. https://doi.org/10.1108/RPJ-04-2017-0055.
[105] H.N. Chia, B.M. Wu, Recent advances in 3D printing of biomaterials, J. Biol. Eng. 9 (2015) 4.
[106] I. Zein, D.W. Hutmacher, K.C. Tan, S.H. Teoh, Fused deposition modeling of novel scaffold architectures for tissue engineering applications, Biomaterials. 23 (2002) 1169–1185. https://doi.org/10.1016/S0142-9612(01)00232-0.
[107] H.-J. Yen, C.-S. Tseng, S. Hsu, C.-L. Tsai, Evaluation of chondrocyte growth in the highly porous scaffolds made by fused deposition manufacturing (FDM) filled with type II collagen, Biomed. Microdevices. 11 (2009) 615–624. https://doi.org/10.1007/s10544-008-9271-7.
[108] A.V. Mironov, A.M. Grigoryev, L.I. Krotova, N.N. Skaletsky, V.K. Popov, V.I. Sevastianov, 3D printing of PLGA scaffolds for tissue engineering, J. Biomed. Mater. Res. A. 105 (2017) 104–109.
[109] J.-H. Shim, J.Y. Kim, J.K. Park, S.K. Hahn, J.-W. Rhie, S.-W. Kang, S.-H. Lee, D.-W. Cho, Effect of Thermal Degradation of SFF-Based PLGA Scaffolds Fabricated Using a Multi-head Deposition System Followed by Change of Cell Growth Rate, J. Biomater. Sci. Polym. Ed. 21 (2010) 1069–1080. https://doi.org/10.1163/092050609X12457428919034.
[110] F. Bignotti, M. Penco, L. Sartore, S. D'Antone, A. D'Amore, G. Spagnoli, Thermal degradation of two classes of block copolymers based on poly(lactic-glycolic acid) and poly(ϵ-caprolactone) or poly(ethylene glycol), Macromol. Symp. 180 (2002) 257–266. https://doi.org/10.1002/1521-3900(200203)180:1<257::AID-MASY257>3.0.CO;2-I.
[111] S.H. Park, D.S. Park, J.W. Shin, Y.G. Kang, H.K. Kim, T.R. Yoon, J.-W. Shin, Scaffolds for bone tissue engineering fabricated from two different materials by the rapid prototyping technique: PCL versus PLGA, J. Mater. Sci. Mater. Med. 23 (2012) 2671–2678. https://doi.org/10.1007/s10856-012-4738-8.
[112] I. Bružauskaitė, D. Bironaitė, E. Bagdonas, E. Bernotienė, Scaffolds and cells for tissue regeneration: different scaffold pore sizes—different cell effects, Cytotechnology. 68 (2016) 355–369. https://doi.org/10.1007/s10616-015-9895-4.
[113] S. Yang, K.-F. Leong, Z. Du, C.-K. Chua, The Design of Scaffolds for Use in Tissue Engineering. Part I. Traditional Factors, Tissue Eng. 7 (2001) 679–689. https://doi.org/10.1089/107632701753337645.
[114] B. Ostrowska, A. Di Luca, K. Szlazak, L. Moroni, W. Swieszkowski, Influence of internal pore architecture on biological and mechanical properties of three-dimensional fiber deposited scaffolds for bone regeneration, J. Biomed. Mater. Res. A. 104 (2016) 991–1001. https://doi.org/10.1002/jbm.a.35637.
[115] S. Naghieh, M.R. Karamooz Ravari, M. Badrossamay, E. Foroozmehr, M. Kadkhodaei, Numerical investigation of the mechanical properties of the additive manufactured bone scaffolds fabricated by FDM: The effect of layer penetration and post-heating, J. Mech. Behav. Biomed. Mater. 59 (2016) 241–250. https://doi.org/10.1016/j.jmbbm.2016.01.031.

[116] N. Rodrigues, M. Benning, A.M. Ferreira, L. Dixon, K. Dalgarno, Manufacture and Characterisation of Porous PLA Scaffolds, Procedia CIRP. 49 (2016) 33–38. https://doi.org/10.1016/j.procir.2015.07.025.
[117] C.E. Corcione, F. Gervaso, F. Scalera, F. Montagna, T. Maiullaro, A. Sannino, A. Maffezzoli, 3D printing of hydroxyapatite polymer-based composites for bone tissue engineering, J. Polym. Eng. 37 (2017) 741–746.
[118] F.S. Senatov, K.V. Niaza, M.Yu. Zadorozhnyy, A.V. Maksimkin, S.D. Kaloshkin, Y.Z. Estrin, Mechanical properties and shape memory effect of 3D-printed PLA-based porous scaffolds, J. Mech. Behav. Biomed. Mater. 57 (2016) 139–148. https://doi.org/10.1016/j.jmbbm.2015.11.036.
[119] J. Lee, H. Lee, K.-H. Cheon, C. Park, T.-S. Jang, H.-E. Kim, H.-D. Jung, Fabrication of poly(lactic acid)/Ti composite scaffolds with enhanced mechanical properties and biocompatibility via fused filament fabrication (FFF)–based 3D printing, Addit. Manuf. 30 (2019) 100883. https://doi.org/10.1016/j.addma.2019.100883.
[120] E. Ceretti, P. Ginestra, P.I. Neto, A. Fiorentino, J.V.L. Da Silva, Multi-layered Scaffolds Production via Fused Deposition Modeling (FDM) Using an Open Source 3D Printer: Process Parameters Optimization for Dimensional Accuracy and Design Reproducibility, Procedia CIRP. 65 (2017) 13–18. https://doi.org/10.1016/j.procir.2017.04.042.
[121] L. Dong, S.-J. Wang, X.-R. Zhao, Y.-F. Zhu, J.-K. Yu, 3D- Printed Poly(ε-caprolactone) Scaffold Integrated with Cell-laden Chitosan Hydrogels for Bone Tissue Engineering, Sci. Rep. 7 (2017) 1–9. https://doi.org/10.1038/s41598-017-13838-7.
[122] H. Chim, D.W. Hutmacher, A.M. Chou, A.L. Oliveira, R.L. Reis, T.C. Lim, J.-T. Schantz, A comparative analysis of scaffold material modifications for load-bearing applications in bone tissue engineering, Int. J. Oral Maxillofac. Surg. 35 (2006) 928–934. https://doi.org/10.1016/j.ijom.2006.03.024.
[123] Z. Xiong, Y. Yan, S. Wang, R. Zhang, C. Zhang, Fabrication of porous scaffolds for bone tissue engineering via low-temperature deposition, Scr. Mater. 46 (2002) 771–776. https://doi.org/10.1016/S1359-6462(02)00071-4.
[124] C.S. Ki, S.Y. Park, H.J. Kim, H.-M. Jung, K.M. Woo, J.W. Lee, Y.H. Park, Development of 3-D nanofibrous fibroin scaffold with high porosity by electrospinning: implications for bone regeneration, Biotechnol. Lett. 30 (2008) 405–410. https://doi.org/10.1007/s10529-007-9581-5.
[125] J. Mendez, P.K. Annamalai, S.J. Eichhorn, R. Rusli, S.J. Rowan, E.J. Foster, C. Weder, Bioinspired Mechanically Adaptive Polymer Nanocomposites with Water-Activated Shape-Memory Effect, Macromolecules. 44 (2011) 6827–6835. https://doi.org/10.1021/ma201502k.
[126] X.-J. Han, Z.-Q. Dong, M.-M. Fan, Y. Liu, J.-H. li, Y.-F. Wang, Q.-J. Yuan, B.-J. Li, S. Zhang, pH-induced shape-memory polymers, Macromol. Rapid Commun. 33 (2012) 1055–1060.
[127] H. Xie, M. He, X.-Y. Deng, L. Du, C.-J. Fan, K.-K. Yang, Y.-Z. Wang, Design of Poly(l-lactide)–Poly(ethylene glycol) Copolymer with Light-Induced Shape-Memory Effect Triggered by Pendant Anthracene Groups, ACS Appl. Mater. Interfaces. 8 (2016) 9431–9439. https://doi.org/10.1021/acsami.6b00704.
[128] H.Y. Jiang, S. Kelch, A. Lendlein, Polymers Move in Response to Light, Adv. Mater. 18 (2006) 1471–1475. https://doi.org/10.1002/adma.200502266.
[129] W. Small IV, T.S. Wilson, W.J. Benett, J.M. Loge, D.J. Maitland, Laser-activated shape memory polymer intravascular thrombectomy device, Opt. Express. 13 (2005) 8204–8213.

[130] X. Yu, S. Zhou, X. Zheng, T. Guo, Y. Xiao, B. Song, A biodegradable shape-memory nanocomposite with excellent magnetism sensitivity, Nanotechnology. 20 (2009) 235702. https://doi.org/10.1088/0957-4484/20/23/235702.
[131] H. Wu, P. Chen, C. Yan, C. Cai, Y. Shi, Four-dimensional printing of a novel acrylate-based shape memory polymer using digital light processing, Mater. Des. 171 (2019) 107704. https://doi.org/10.1016/j.matdes.2019.107704.
[132] W. Small IV, P. Singhal, T.S. Wilson, D.J. Maitland, Biomedical applications of thermally activated shape memory polymers, J. Mater. Chem. 20 (2010) 3356–3366.
[133] M. Behl, A. Lendlein, Shape-memory polymers, Mater. Today. 10 (2007) 20–28. https://doi.org/10.1016/S1369-7021(07)70047-0.
[134] S. Miao, N. Castro, M. Nowicki, L. Xia, H. Cui, X. Zhou, W. Zhu, S. Lee, K. Sarkar, G. Vozzi, Y. Tabata, J. Fisher, L.G. Zhang, 4D printing of polymeric materials for tissue and organ regeneration, Mater. Today. 20 (2017) 577–591. https://doi.org/10.1016/j.mattod.2017.06.005.
[135] S.A. Abdullah, A. Jumahat, N.R. Abdullah, L. Frormann, Determination of Shape Fixity and Shape Recovery Rate of Carbon Nanotube-filled Shape Memory Polymer Nanocomposites, Procedia Eng. 41 (2012) 1641–1646. https://doi.org/10.1016/j.proeng.2012.07.362.
[136] L. Xue, S. Dai, Z. Li, Biodegradable shape-memory block co-polymers for fast self-expandable stents, Biomaterials. 31 (2010) 8132–8140. https://doi.org/10.1016/j.biomaterials.2010.07.043.
[137] C. Liu, H. Qin, P.T. Mather, Review of progress in shape-memory polymers, J. Mater. Chem. 17 (2007) 1543–1558.
[138] Y.-C. Sun, S. Cai, J. Ren, H. E. Naguib, Room temperature deformable shape memory composite with fine-tuned crystallization induced via nanoclay particles, J. Polym. Sci. Part B Polym. Phys. 55 (2017) 1197–1206.
[139] J. Karger-Kocsis, S. Kéki, Biodegradable polyester-based shape memory polymers: Concepts of (supra) molecular architecturing, Express Polym. Lett. 8 (2014) 397–412.
[140] V. Sessini, J.-M. Raquez, G. Lo Re, R. Mincheva, J.M. Kenny, P. Dubois, L. Peponi, Multiresponsive Shape Memory Blends and Nanocomposites Based on Starch, ACS Appl. Mater. Interfaces. 8 (2016) 19197–19201. https://doi.org/10.1021/acsami.6b06618.
[141] W. Sokolowski, A. Metcalfe, S. Hayashi, J. Raymond, Medical applications of shape memory polymers, Biomed. Mater. 2 (2007) S23.
[142] H.-Y. Mi, X. Jing, B.N. Napiwocki, B.S. Hagerty, G. Chen, L.-S. Turng, Biocompatible, degradable thermoplastic polyurethane based on polycaprolactone-block-polytetrahydrofuran-block-polycaprolactone copolymers for soft tissue engineering, J. Mater. Chem. B. 5 (2017) 4137–4151.
[143] S.K. Dogan, S. Boyacioglu, M. Kodal, O. Gokce, G. Ozkoc, Thermally induced shape memory behavior, enzymatic degradation and biocompatibility of PLA/TPU blends: "Effects of compatibilization," J. Mech. Behav. Biomed. Mater. 71 (2017) 349–361. https://doi.org/10.1016/j.jmbbm.2017.04.001.
[144] S.-M. Lai, Y.-C. Lan, Shape memory properties of melt-blended polylactic acid (PLA)/thermoplastic polyurethane (TPU) bio-based blends, J. Polym. Res. 20 (2013) 140.
[145] X. Zheng, S. Zhou, X. Li, J. Weng, Shape memory properties of poly(d,l-lactide)/hydroxyapatite composites, Biomaterials. 27 (2006) 4288–4295. https://doi.org/10.1016/j.biomaterials.2006.03.043.
[146] W. Zhang, L. Chen, Y. Zhang, Surprising shape-memory effect of polylactide resulted from toughening by polyamide elastomer, Polymer. 50 (2009) 1311–1315.

[147] A.B. Kutikov, K.A. Reyer, J. Song, Shape-Memory Performance of Thermoplastic Amphiphilic Triblock Copolymer Poly(d,l-lactic acid-co-ethylene glycol-co-d,l-lactic acid) (PELA)/Hydroxyapatite Composites, Macromol. Chem. Phys. 215 (2014) 2482–2490. https://doi.org/10.1002/macp.201400340.
[148] T. Shen, M. Lu, D. Zhou, L. Liang, Influence of blocked polyisocyanate on thermomechanical, shape memory and biodegradable properties of poly (lactic acid)/poly (ethylene glycol) blends, Iran. Polym. J. 21 (2012) 317–323.
[149] Y. Guo, J. Ma, Z. Lv, N. Zhao, L. Wang, Q. Li, The effect of plasticizer on the shape memory properties of poly(lactide acid)/poly(ethylene glycol) blends, J. Mater. Res. 33 (2018) 4101–4112. https://doi.org/10.1557/jmr.2018.359.
[150] S. Cai, Y.-C. Sun, J. Ren, H.E. Naguib, Toward the low actuation temperature of flexible shape memory polymer composites with room temperature deformability via induced plasticizing effect, J. Mater. Chem. B. 5 (2017) 8845–8853. https://doi.org/10.1039/C7TB02068F.
[151] W. Koosomsuan, M. Yamaguchi, P. Phinyocheep, K. Sirisinha, High-Strain Shape Memory Behavior of PLA–PEG Multiblock Copolymers and Its Microstructural Origin, J. Polym. Sci. Part B Polym. Phys. 57 (2019) 241–256. https://doi.org/10.1002/polb.24775.
[152] G.I. Peterson, A.V. Dobrynin, M.L. Becker, Biodegradable shape memory polymers in medicine, Adv. Healthc. Mater. 6 (2017) 1700694.
[153] F.S. Senatov, M.Yu. Zadorozhnyy, K.V. Niaza, V.V. Medvedev, S.D. Kaloshkin, N.Y. Anisimova, M.V. Kiselevskiy, K.-C. Yang, Shape memory effect in 3D-printed scaffolds for self-fitting implants, Eur. Polym. J. 93 (2017) 222–231. https://doi.org/10.1016/j.eurpolymj.2017.06.011.
[154] W.J. Hendrikson, J. Rouwkema, F. Clementi, C.A. van Blitterswijk, S. Farè, L. Moroni, Towards 4D printed scaffolds for tissue engineering: exploiting 3D shape memory polymers to deliver time-controlled stimulus on cultured cells, Biofabrication. 9 (2017) 031001. https://doi.org/10.1088/1758-5090/aa8114.

Material's features

Biocompatibility
Bioactivity
Biodegradability
…

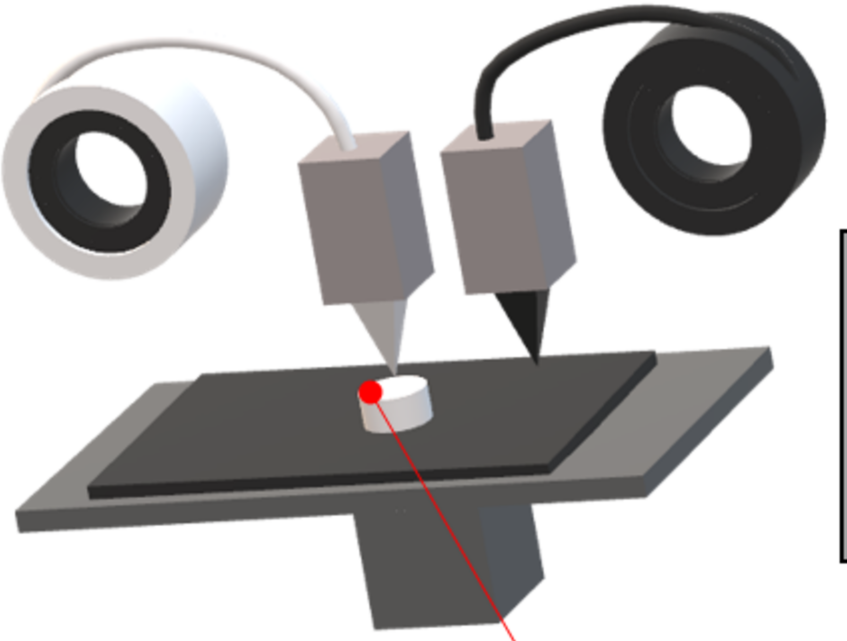

FFF settings

Temperatures
Layer thickness
Deposition angles
Filling rate
Build orientation
…

3D printing (FFF) of scaffolds

Scaffold properties

Pore size
Porosity
Mechanical properties
Microstructure
Shape-memory
Behavior *in vivo*
…